# Influence of anthropogenic sulfate and black carbon on upper tropospheric clouds in the NCAR CAM3 model coupled to the IMPACT global aerosol model

Xiaohong Liu,[1] Joyce E. Penner,[2] and Minghuai Wang[2]

Received 27 May 2008; revised 25 August 2008; accepted 10 November 2008; published 11 February 2009.

[1] The influence of anthropogenic aerosol (sulfate and soot) on upper tropospheric (UT) clouds through ice nucleation is studied using the NCAR Community Atmospheric Model Version 3 (CAM3) with a double moment ice microphysics treatment coupled to a global aerosol model (LLNL/UMich IMPACT). Present-day and preindustrial simulations are performed and compared for two scenarios. In the first scenario, the homogeneous freezing of sulfate particles dominates cirrus cloud formation in the upper troposphere (HOM). In the second scenario, both homogeneous and heterogeneous ice nucleation and their competition (HET) are allowed. In the HOM scenario, anthropogenic sulfate results in a global annual mean change of long-wave cloud forcing (LWCF) of $0.20 \pm 0.09$ W m$^{-2}$ and short-wave cloud forcing (SWCF) of $0.30 \pm 0.17$ W m$^{-2}$ and an increase of upper tropospheric/lower stratospheric (UT/LS) water vapor by $\sim$10%. In the HET scenario, anthropogenic soot may increase global cirrus cloud cover by $\sim$2% and UT/LS water vapor by 40% with a change in LWCF of 1.5 W m$^{-2}$ (with $1.35 \pm 0.15$ W m$^{-2}$ from surface soot and $0.12 \pm 0.17$ W m$^{-2}$ from aircraft soot) if soot acts as efficient ice nuclei (IN) with a threshold ice nucleation $RH_i$ of 120–130%. Aerosol effects are most evident (larger than natural variability) over polar regions. However, their influence is significantly reduced if soot has a threshold $RH_i$ of 140% with an LWCF change of only 0.23 W m$^{-2}$ (with $0.17 \pm 0.18$ W m$^{-2}$ from surface soot and $0.06 \pm 0.16$ W m$^{-2}$ from aircraft soot), and cloud forcing changes are statistically insignificant (less than the natural variability). Our results reinforce the importance of understanding ice nucleation on soot from the perspective of their global climate impact.

**Citation:** Liu, X., J. E. Penner, and M. Wang (2009), Influence of anthropogenic sulfate and black carbon on upper tropospheric clouds in the NCAR CAM3 model coupled to the IMPACT global aerosol model, *J. Geophys. Res.*, *114*, D03204, doi:10.1029/2008JD010492.

## 1. Introduction

[2] Upper tropospheric cirrus clouds cover about 30% of the earth's surface [*Wang et al.*, 1996; *Rossow and Schiffer*, 1999]. The formation of cirrus clouds and the effect of changes in aerosols on the climate forcing associated with cirrus remains one of the least understood processes in the climate system, although it is generally accepted that cirrus clouds play an important role in determining the earth's radiative budget and climate [*Liou*, 1986; *Ramanathan and Collins*, 1991]. Tropical cirrus clouds may also influence the water vapor content in the stratosphere through dehydration processes [e.g., *Jensen et al.*, 2001].

[3] Ice crystal nucleation involves a variety of mechanisms, each of which involves aerosol particles or cloud droplets condensed on aerosol particles. There are two main classes of mechanisms: homogeneous and heterogeneous. Homogeneous nucleation involves homogeneous freezing of supercooled cloud or haze droplets at temperatures less than −37°C. Heterogeneous mechanisms include direct deposition from vapor to ice on a suitable nucleus (deposition nucleation) and freezing of previously condensed supercooled cloud or haze droplets, with the freezing initiated either by contact of a nuclei with the cloud or haze droplet (contact nucleation) or by a nuclei immersed within the cloud or haze droplet (immersion nucleation) and generally require lower relative humidity over ice ($RH_i$) than homogeneous freezing. Mineral dust, carbonaceous and metallic particles appear to be common heterogeneous ice nuclei (IN [*Chen et al.*, 1998; *DeMott et al.*, 2003; *Cziczo et al.*, 2004]), while aqueous sulfate drops are thought to be the most important homogeneous nuclei. Because of the lower $RH_i$ required for ice nucleation, the presence of heterogeneous IN could decrease the occurrence of homogeneous nucleation due to the consumption of water vapor by ice crystals formed from heterogeneous nucleation [e.g., *DeMott et al.*, 1997]. However, the relative importance of homogeneous nucle-

[1] Atmospheric Science and Global Change Division, Pacific Northwest National Laboratory, Richland, Washington, USA.
[2] Department of Atmospheric, Oceanic and Space Sciences, University of Michigan, Ann Arbor, Michigan, USA.


0148-0227/09/2008JD010492

ation versus heterogeneous nucleation for cirrus cloud formation has been debated for years [*Pruppacher and Klett*, 1997; *Haag and Kärcher*, 2004] because of a shortage of information on the concentrations and properties of IN in the upper troposphere.

[4] The global burdens of sulfate and carbonaceous aerosols have substantially increased from preindustrial times to the present day, raising the possibility of an indirect aerosol effect on cirrus clouds. In situ measurements during the Interhemispheric Differences in Cirrus Properties from Anthropogenic Emissions (INCA) campaign indicate that the occurrence of very high supersaturation with respect to ice varies significantly between the Northern and Southern hemispheres, and these differences are attributed to increased aerosols at Northern latitudes [*Haag et al.*, 2003]. Aircraft exhaust, which contains black carbon soot, volatile particles, and metallic particles, can directly form contrails [*Schumann*, 2002] and may indirectly change the ice crystal number concentration of natural ice clouds [*Ström and Ohlsson*, 1998], with a possible regional climate impact [*Travis et al.*, 2002]. Surface-generated soot may similarly affect cirrus clouds.

[5] Process modeling studies have suggested that optically thin and subvisible cirrus generated in situ are particularly susceptible to heterogeneous IN near the tropical tropopause [*Kärcher*, 2004]. The frequency of occurrence of thin cirrus can be significantly increased due to the presence of a small number of IN (0.001 $cm^{-3}$) at midlatitudes as shown in Lagrangian microphysical aerosol-cloud model simulations [*Haag and Kärcher*, 2004]. If cirrus cloud occurrence frequency and microphysical characteristics (such as ice crystal number density, size, and shape) are modified by human-related activities, this could have a large influence on the radiative feedback of these clouds [*Stephens et al.*, 1990; *Smith et al.*, 1998]. The size of ice crystals determines their sedimentation velocity and therefore the cloud lifetime and the humidity of the upper troposphere and lower stratosphere [e.g., *Jensen et al.*, 2001; *Jensen and Pfister*, 2004; *Sherwood*, 2002]. Recent indications that stratospheric water vapor concentrations are changing [*Nedoluha et al.*, 2003; *Rosenlof et al.*, 2001; *Oltmans et al.*, 2000] have intensified the urgency of understanding the processes controlling water vapor in the tropical tropopause layer (TTL).

[6] In recent years physically based parameterizations for the homogeneous freezing of sulfate solution droplets and for heterogeneous immersion freezing in cirrus formation have been developed [*Kärcher and Lohmann*, 2002a, 2002b; *Liu and Penner*, 2005; *Kärcher et al.*, 2006]. These parameterizations link the number of ice crystals that nucleate to air temperature, updraft velocity and aerosol properties (e.g., number and size), and thereby allow the simulation of the impacts of different ice nucleation mechanisms on cirrus clouds and climate. Using parameterizations implemented in the ECHAM GCM, *Lohmann and Kärcher* [2002] simulated cirrus clouds formed by homogeneous freezing while *Lohmann et al.* [2004] studied the effects of heterogeneous freezing on cirrus clouds.

[7] *Liu et al.* [2007a, hereafter as LIU07] implemented the ice nucleation parameterization by *Liu and Penner* [2005] into the National Center for Atmospheric Research (NCAR) Community Atmospheric Model Version 3 (CAM3) by introducing a prognostic equation for cloud ice number concentration (a two-moment method). The cloud liquid conversion to cloud ice in mixed-phase clouds (Bergeron-Findeisen process) is also explicitly considered by replacing the temperature-dependent cloud phase partitioning in the standard CAM3 with the *Rotstayn et al.* [2000] scheme. The *Liu and Penner* [2005] parameterization accounts for homogeneous nucleation (on sulfate particles) and heterogeneous immersion nucleation (on soot particles), heterogeneous deposition nucleation, and considers the competition between these mechanisms. However, since our dust number concentration in the upper troposphere is small [*Penner et al.*, 2008], the influence of dust on ice concentrations in cirrus is neglected, but dust is allowed to affect ice nucleation in mixed-phase clouds through the contact freezing of cloud droplets. The predicted cloud ice water content (IWC) in the upper troposphere from LIU07 is in better agreement with the Aura Microwave Limb Sounder (MLS) data than that from the standard CAM3 and the predicted tropopause temperatures are also improved. It was also shown that this ice scheme is able to produce a more realistic simulation of the cloud phase structure and the partitioning of condensed water into liquid droplets during the Mixed-Phase Arctic Cloud Experiment (M-PACE) than the standard CAM3 when tested in a single column model [*Liu et al.*, 2007b] and in a short-range weather forecasting approach [*Xie et al.*, 2008].

[8] This work is a follow-up to LIU07, studying the potential influences of anthropogenic aerosol (sulfate and soot) on upper tropospheric cirrus and water vapor through ice nucleation using the modified version of CAM3 with ice nucleation in LIU07 coupled to the IMPACT global aerosol model (M. Wang et al., The coupled IMPACT aerosol and NCAR CAM3 model: Evaluation of aerosol fields and analysis of uncertainties with simulated aerosol number and size, submitted to *Journal of Geophysical Research*, 2008, hereinafter referred to as Wang et al., submitted manuscript, 2008). Two scenarios are considered: only homogeneous ice nucleation (HOM) and both homogeneous and heterogeneous ice nucleation (HET). In HET, the sensitivity to the heterogeneous immersion nucleation relative humidity threshold ($RH_i$) and to the critical heterogeneous IN number concentration that determines the transition from homogeneous to heterogeneous nucleation is studied. The indirect cloud forcing (for cirrus clouds only) associated with anthropogenic sulfate and soot from surface sources (fossil fuel and biomass burning) and from aviation is calculated.

[9] The paper is organized as follows. The coupled models are described in section 2. The influence of anthropogenic aerosols through ice nucleation on both cirrus clouds and water vapor concentrations and uncertainties due to heterogeneous ice nucleation are presented in section 3. Section 4 describes the cirrus cloud radiative forcing calculated for individual aerosol components (anthropogenic sulfate and soot from both surface and aircraft sources). Section 5 summarizes and concludes this study.

## 2. Model Description

### 2.1. NCAR CAM3

[10] The NCAR CAM3 is the atmospheric component of the Community Climate System Model (CCSM [*Collins et al.*, 2006]). The treatment of cloud condensation and

microphysics in CAM3 is based on the work of *Rasch and Kristjánsson* [1998] as updated by *Zhang et al.* [2003] with separate prognostic equations for the liquid and ice-phase condensate [*Boville et al.*, 2006]. Even though each phase of water is transported separately, after advection, convective detrainment, and sedimentation, liquid and ice are repartitioned according to a temperature-dependent fraction of ice in total water ($f_i$)

$$0 \le f_i = \frac{T - T_{\max}}{T_{\min} - T_{\max}} \le 1, \quad (1)$$

where the bounds $T_{\min}$ and $T_{\max}$ are adjustable within a narrow range. The values in CAM3 are $-40$°C and $-10$°C, respectively. Therefore CAM3 is not able to represent a variety of processes (e.g., the Bergeron-Findeisen process, ice nucleation, etc.) in mixed-phase clouds. The standard CAM3 has been extensively evaluated by comparison with observations. *Hack et al.* [2006] and *Boville et al.* [2006] compared water vapor and temperature from CAM3 to reanalysis data and to radiosonde measurements. Upper tropospheric water vapor from CAM3 was also evaluated with satellite observations by *Gettelman et al.* [2006].

[11] A two-moment cloud microphysics scheme was introduced into the CAM3 model in LIU07, in which cloud liquid and cloud ice number concentration are predicted. The liquid and ice mixing ratio is calculated by the modified *Rasch and Kristjánsson* [1998] scheme described by *Boville et al.* [2006] except that the liquid mass conversion to ice due to the depositional growth of cloud ice at the expense of liquid water (the Bergeron-Findeisen process) is explicitly treated using the *Rotstayn et al.* [2000] scheme. Moreover, the cloud condensation and evaporation (C-E) scheme of *Rasch and Kristjánsson* [1998], which removes ice supersaturation for ice clouds in the standard CAM3, was used only for liquid water in warm and mixed-phase clouds. We added vapor deposition and sublimation of cirrus cloud ice based on the *Rotstayn et al.* [2000] scheme. With these modifications, ice supersaturation was allowed in the upper troposphere. Thus rather than simply diagnosing the condensate phase from temperature as in equation (1), LIU07 has a physically based representation of the liquid/ice partitioning in mixed-phase clouds as well as the capability to predict ice supersaturation.

[12] LIU07 has included a comparison between the modified and standard CAM3 for water vapor, temperature, cloud fields (condensate mixing ratio, cloud cover, cloud forcing, etc.) in their Figure 7 and Table 3. Changes in temperature are less than 0.5°C except in the tropical tropopause where temperature increases by 1–2°C due to the increase in ice mixing ratios, which reduces the standard CAM3 cold bias there. Changes in water vapor are less than a few percent except in the tropical tropopause and lower stratosphere above 200 hPa where water vapor increases by ~40% due to the temperature increase in the tropical tropopause allowing more water vapor transported into the stratosphere (note that the absolute amount change is much smaller than that in the boundary layer).

[13] The statistics for the predicted $RH_i$ in the UT/LS region in this modified version of the CAM3 was compared with the Measurement of Ozone on Airbus In-Service Aircraft (MOZAIC) data within flight tracks as shown in Figure 3 of LIU07. The occurrence frequency of ice supersaturation at 200–300 hPa and 300–500 hPa is underestimated in CAM3, which is possibly due to the large grid size (2.5° × 2°). It is closer to measured supersaturations from the Atmospheric Infrared Sounder (AIRS) (A. Gettelman, personal communication, 2007). This points out the importance of a treatment for the subgrid variability of the RH. Below, we perform a sensitivity test in which we add 20% to the calculated $RH_i$ in determining the number of ice crystals nucleated. We note that the stratiform cloud fraction was calculated using the same RH-based formulation with the same threshold RH value as that in the standard CAM3 model. Since we allowed ice supersaturation in LIU07, this produced a larger high-cloud fraction in the tropics and extratropics compared to that in the standard CAM3.

[14] Another important change to CAM3 introduced in LIU07 is that the effective radius of cloud ice is calculated from model-predicted mass and number rather than prescribed as a function of temperature as in the standard CAM3. This, together with a parameterization of ice nucleation, allows us to study the effects of aerosols on cloud radiative forcing and cloud particle sedimentation through their influence on the number and size of cloud particles (and thus their effective radii). This is the main focus of this study. For the purpose of studying only the effects of adding ice microphysics, we turned off the aerosol effect on liquid water clouds developed by Wang et al. (submitted manuscript, 2008) by using the prescribed droplet effective radius in the standard CAM3 [*Boville et al.*, 2006]. We note that there are a few global models that include discrete size-resolved treatment of cloud microphysical processes [e.g., *Jacobson*, 2003]. As also summarized by *Zhang* [2008], the original version of CAM3 is still missing several treatments of aerosol properties and processes, and cloud microphysics and aerosol-chemistry-cloud interactions which need to be improved in future versions of CAM.

[15] Ice nucleation mechanisms in LIU07 include homogeneous ice nucleation and heterogeneous immersion nucleation in ice clouds with temperature less than $-35$°C [*Liu and Penner*, 2005], contact freezing of cloud droplets through Brownian coagulation with insoluble IN (assumed to be mineral dust with radii large than 0.63 $\mu$m, i.e., the largest 3 dust size bins in the model [*Young*, 1974]), and deposition/condensation nucleation [*Meyers et al.*, 1992] in mixed-phase clouds. Secondary ice production by ice splintering between $-3°$ and $-8$°C is included using the Hallet-Mossop scheme. Evaporation freezing of droplets in mixed-phase clouds is not treated because of uncertainties in the extent of this freezing that might take place in mixed-phase clouds [*Heymsfield et al.*, 2005]. The *Liu and Penner* [2005] parameterization represents the competition between homogeneous and heterogeneous nucleation pathways. It is assumed that sulfate particles form ice through homogeneous freezing after deliquescence [*Koop et al.*, 2000]. The ice nuclei for immersion nucleation is assumed to be soot particles since soot particles are often internally mixed with soluble species (e.g., sulfate) due to aging in the atmosphere [e.g., *Murphy et al.*, 2006]. Single particle measurements found that dust particles are generally insoluble and have little soluble compounds associated with them [*Cziczo et al.*, 2004]. Thus we assume that they can act as contact IN for cloud droplet freezing [*Lohmann*, 2002], and as deposition/

condensation IN as represented by the *Meyers et al.* [1992] parameterization (we scaled the Meyers et al.'s formula with a vertical decay function obtained for refractory aerosols in the INCA [*Minikin et al.*, 2003]). This study focuses on the influence of anthropogenic aerosols (sulfate and soot) on cirrus clouds. Mineral dust emissions are assumed constant between preindustrial and present-day conditions.

[16] While there is a good understanding of ice nucleation through the homogeneous freezing of sulfate [*Sassen and Dodd*, 1988; *Koop et al.*, 2000], there are large differences reported for the nucleation efficiency of soot particles [*DeMott*, 1990; *DeMott et al.*, 1999; *Möhler et al.*, 2005a, 2005b; *Dymarska et al.*, 2006]. *Liu and Penner* [2005] derived a threshold relative humidity with respective to water ($RH_w$) for immersion nucleation using the classical theory for ice nucleation and a value of 0.5 for the compatibility parameter $m_{is}$ (cosine of the contact angle between the ice germ and solid substrate [*Pruppacher and Klett*, 1997]), which was represented as

$$RH_w(\%) = 0.0073\ T^2 + 1.477\ T + 131.74. \quad (2)$$

Accordingly, the threshold $RH_i$ is rather insensitive to the temperature and is of order 120–130% for the temperature range between −40 and −80°C, close to recent laboratory data for soot by *Möhler et al.* [2005a]. To examine the effects of uncertainties in the heterogeneous ice nucleation threshold $RH_i$ for soot particles, we performed a sensitivity test which used a threshold $RH_i$ of 140% to represent a scenario with less efficient nucleation on soot particles [*Dymarska et al.*, 2006; *DeMott et al.*, 1999; *Möhler et al.*, 2005b].

[17] Model simulations have shown that homogeneous nucleation starts later in the presence of heterogeneous IN, and, as a result, ice number concentrations are decreased due to the competition between heterogeneous and homogeneous nucleation as compared to a pure homogeneous nucleation mechanism [*DeMott et al.*, 1997]. As indicated by *Kärcher et al.* [2006], the transition from the pure heterogeneous nucleation regime to the homogeneous-dominated regime occurs over an order of magnitude in vertical velocities. *Liu and Penner* [2005] derived the critical IN number concentration $N_{s,c}$ (in units of $cm^{-3}$) above which only heterogeneous ice nucleation occurs as

$$N_{s,c} = \exp\left\{\frac{12.884 \ln w - 67.69 - T}{1.4938 \ln w + 10.41}\right\}. \quad (3)$$

$N_{s,c}$ calculated from equation (3) is comparable to that from the formulation of *Gierens* [2003] when the updraft velocity is higher than 0.2 m $s^{-1}$ but is much less when the updraft velocity is lower than 0.1 m $s^{-1}$. Thus a second sensitivity test is performed using the *Gierens* [2003] formulation with a higher critical IN number concentration for heterogeneous nucleation. *Liu and Penner* [2005] allowed an order of magnitude of transition in the IN soot number. For soot number less than $N_{s,c}/10$, we assumed that ice number from pure homogeneous nucleation is used. For soot number between $N_{s,c}/10$ and $N_{s,c}$, the ice number $N_i$ is interpolated in-between that for homogeneous nucleation only and that for heterogeneous nucleation only.

[18] Aircraft measurements of cirrus clouds at midlatitudes and in the tropics suggest that there is ubiquitous mesoscale variability driven by high frequency gravity waves [*Jensen and Pfister*, 2004; *Hoyle et al.*, 2005; *Haag and Kärcher*, 2004]. The averages of the probability distributions of temperature fluctuations correspond to cooling rates on the order of 10 K $h^{-1}$ (or updraft velocities on the order of 20–30 cm $s^{-1}$). To account for these small-scale temperature fluctuations which are currently unresolved in global models, but are very important in ice nucleation we included in LIU07 an assumed subgrid scale variation of the updraft velocity. This is modeled by adding a Gaussian distribution with a standard deviation of 25 cm $s^{-1}$ to the large scale updraft velocity predicted by the climate model. We note that more measurements of updraft velocities in different types of cirrus clouds are needed in order to better represent this variability.

### 2.2. The IMPACT Global Aerosol Model

[19] The Lawrence Livermore National Laboratory (LLNL)/University of Michigan IMPACT model is used in this study to predict the global distribution of atmospheric aerosols [*Liu et al.*, 2005; Wang et al., submitted manuscript, 2008]. The model includes prognostic variables for sulfur and related species: dimethylsulfide (DMS), sulfur dioxide ($SO_2$), sulfate aerosol ($SO_4^{2-}$) and hydrogen peroxide ($H_2O_2$); biomass burning black carbon (BC) and organic matter (OM), fossil fuel BC and OM, natural OM, aircraft BC (soot), mineral dust, and sea salt. Sulfate aerosol is divided into three size bins with radii varying from 0.01–0.05 $\mu$m, 0.05–0.63 $\mu$m and 0.63–1.26 $\mu$m, while mineral dust and sea salt are predicted in four bins with radii varying from 0.05–0.63 $\mu$m, 0.63–1.26 $\mu$m, 1.26–2.5 $\mu$m, and 2.5–10 $\mu$m. Carbonaceous aerosol (OM and BC) is currently represented by a single submicron size bin. Emissions of primary particles and precursor gases, gas-phase oxidation of precursor gases, aqueous-phase chemistry, rainout and washout, gravitational settling, and dry deposition are treated. The IMPACT aerosol model driven by meteorological fields from the NASA Data Assimilation Office (DAO) has participated in the AEROCOM (http://nansen.ipsl.jussieu.fr/AEROCOM/) phase A and B evaluations [*Kinne et al.*, 2006; *Textor et al.*, 2006; *Schulz et al.*, 2006], where it has been extensively compared with *in situ* and remotely sensed data for different aerosol properties.

[20] In the current version of the IMPACT model, aerosol (sulfate and soot) number concentrations used in the ice nucleation parameterization are calculated by assuming aerosol size distributions (geometric mode radius and standard deviation) derived from measurements typical of upper tropospheric conditions. Sulfate particles are assumed to have a lognormal size distribution with a mode radius $r_0$ of 0.02 $\mu$m and a distribution width $\sigma$ of 2.3 [*Jensen et al.*, 1994]. For soot particles emitted from the Earth's surface (e.g., biomass burning and fossil fuel combustion), we assumed a size distribution with a mode radius $r_0$ of 0.07 $\mu$m and a distribution width $\sigma$ of 1.5 [*Pueschel et al.*, 1992]. Aircraft soot has a much smaller size with mode radius $r_0$ of 0.023 $\mu$m and a distribution width $\sigma$ of 1.5 [*Petzold and Schröder*, 1998], consistent with measurements showing that BC emitted from surface sources has a much larger fraction of larger BC particles (accumulation mode

size range) than BC emitted from the aircraft at cruise altitudes [*Petzold et al.*, 1999].

[21] We coupled the IMPACT aerosol model with the CAM3 model using MPH (the Multicomponent Handshaking Library; Wang et al., submitted manuscript, 2008). The two model components of the coupled system (hereafter CAM-IMPACT) are concurrently run in MPMD (Multiple Processors Multiple Data) to provide feedbacks between aerosol concentrations and their effects on ice and variables in the climate model (e.g., air temperatures, water vapor, cloud fraction, cloud ice mass mixing ratio, radiation, etc.). A detailed description of the aerosol fields simulated from the CAM-IMPACT model and an evaluation with observations is given in Wang et al. (submitted manuscript, 2008).

## 3. Model Results

[22] Model simulations with the modified CAM3 model (LIU07) coupled to the IMPACT aerosol model were conducted with both present-day (PD) and preindustrial (PI) emissions at $2^\circ \times 2.5^\circ$ horizontal resolution with 26 vertical levels over a period of 5 years after an initial spin-up of 4 months. Climatological sea surface temperatures (SSTs) from 1950–2000 were used. Results from the last 5 years are presented. PD emissions for the aerosol model include fossil fuel $SO_2$ by *Smith et al.* [2004] (with 61.3 Tg S $a^{-1}$), fossil fuel and biomass burning carbonaceous aerosols by *Ito and Penner* [2005] (15.7 Tg OM and 5.8 Tg BC $a^{-1}$ from fossil fuel combustion and 47.4 Tg OM and 4.7 Tg BC $a^{-1}$ from biomass burning), and aircraft soot emissions for 1992 (0.0059 Tg C $a^{-1}$ derived from the aviation fuel use scenario by *Baughcum et al.* [1996] together with a soot emission index of 0.4 g $kg^{-1}$). PI emissions include fossil fuel $SO_2$ for 1850 (1.51 Tg S $a^{-1}$ from the work of *Smith et al.*, 2004), and fossil fuel and biomass burning carbonaceous emissions for 1870 from the work of *Ito and Penner* [2005] (5.09 Tg OM and 0.77 Tg BC $a^{-1}$ from fossil fuel combustion, and 17.9 Tg OM and 1.75 Tg BC $a^{-1}$ from biomass burning). Natural emissions include volcanic emissions of $SO_2$ (4.79 Tg S $a^{-1}$ from the work of *Andres and Kasgnoc*, 1998), dimethyl sulfide (DMS) from the oceans (26.1 Tg S $a^{-1}$ from the work of *Kettle and Andreae*, 2000), natural OM from vegetation (taken to be 9% of the terpene emissions by *Guenther et al.*, 1995 totaling 14.5 Tg $a^{-1}$) and are constant in the PD and PI simulations. Sea salt emissions are calculated online in the coupled model using the method defined by *Gong et al.* [1997] and 10 m wind speeds from CAM3. The 10 m wind speeds are interpolated from a logarithmic profile in CAM3 with a bottom layer thickness of about 100 m. In this paper, the online dust emissions were turned off because the seasonal variation of dust concentrations near the Sahara desert were not correctly represented which may be due to the surface wind simulation at this location in CAM3. Instead, we used the dust emission fluxes at every 6 hours provided by Ginoux (private communication, 2004) for the year 1998 based on the algorithm of *Ginoux et al.* [2001] with a total emission of 2396 Tg $a^{-1}$.

[23] Two scenarios are considered for the pair of PD and PI simulations: in the first scenario we assume that ice nucleation in cirrus clouds is dominated by homogeneous nucleation (simulation HOM). For this we turn off heterogeneous ice nucleation in the *Liu and Penner* [2005] parameterization. In the second scenario heterogeneous nucleation is turned on allowing competition between homogeneous and heterogeneous ice nucleation (simulation HET).

### 3.1. Global Distribution of Sulfate and Soot Aerosol Concentrations

[24] The anthropogenic component of sulfate and carbonaceous aerosols has substantially increased the global mean aerosol burden from preindustrial times to the present. The global annual mean sulfate burden calculated from the coupled CAM-IMPACT model increases from 0.29 Tg S in the preindustrial simulation to 0.72 Tg S in the present-day simulation. The global annual mean burden of BC emitted from surface sources increases from 0.038 Tg to 0.16 Tg and the BC burden from aviation is 0.00031 Tg.

[25] Figure 1 shows a comparison of the present-day sulfate and BC concentrations with those in the preindustrial simulation obtained from the coupled model. Sulfate and BC concentrations increase by more than a factor of 3 in the Northern Hemisphere (NH) midlatitudes and extratropical upper troposphere (at 300–400 hPa). Anthropogenic sulfate and BC are transported toward the southern hemispheric (SH) upper troposphere via the large scale circulation, resulting an increase of sulfate concentration in the SH (at 200–400 hPa) by a factor of $\sim$2 and increase of the BC concentration by more than a factor of 3. In the tropical upper troposphere the sulfate increase is less prominent than that of BC due to the more efficient wet removal of sulfate in deep convective clouds. The BC increase in the tropical upper troposphere depends on the wet removal and thus the hygroscopicity of BC. In the model we assumed a lower BC scavenging efficiency (with a value of 0.3) than that of sulfate (with a value of 1.0). Clearly these changes in sulfate and BC concentrations may have important implications for upper tropospheric clouds (cloud ice number, IWC and cloud fraction) via ice nucleation on these aerosols, which may further impact water vapor, air temperature, etc., through climate feedbacks.

[26] Figure 2 shows the annual average zonal mean BC mass and number concentrations from anthropogenic surface sources (PD minus PI) and from aircraft. The zonal mean BC concentrations from surface anthropogenic sources for the pressure range between 200 and 300 hPa in the NH vary from 1 to 10 ng $m^{-3}$. The maximum zonal mean contributions from aircraft to the BC mass concentration ranges from 0.1 to 1 ng $m^{-3}$ and occur in the NH midlatitude and high latitude UT/LS (in the layer between 100 and 400 hPa). These perturbations are in the same ranges as those documented by *Danilin et al.* [1998] and *Rahmes et al.* [1998], and are larger than the values reported by *Hendricks et al.* [2004] which were 0.01–0.05 ng $m^{-3}$. The calculated percentage contribution of aircraft to the total BC mass concentration is generally less than 10% in the NH midlatitude and high latitude UT/LS, which is consistent with results from the work of *Hendricks et al.* [2004]. The number concentrations of surface BC and aircraft BC are calculated from mass concentrations using surface and aircraft soot size distributions derived from measurements (section 2.2). The zonal mean BC number concentrations

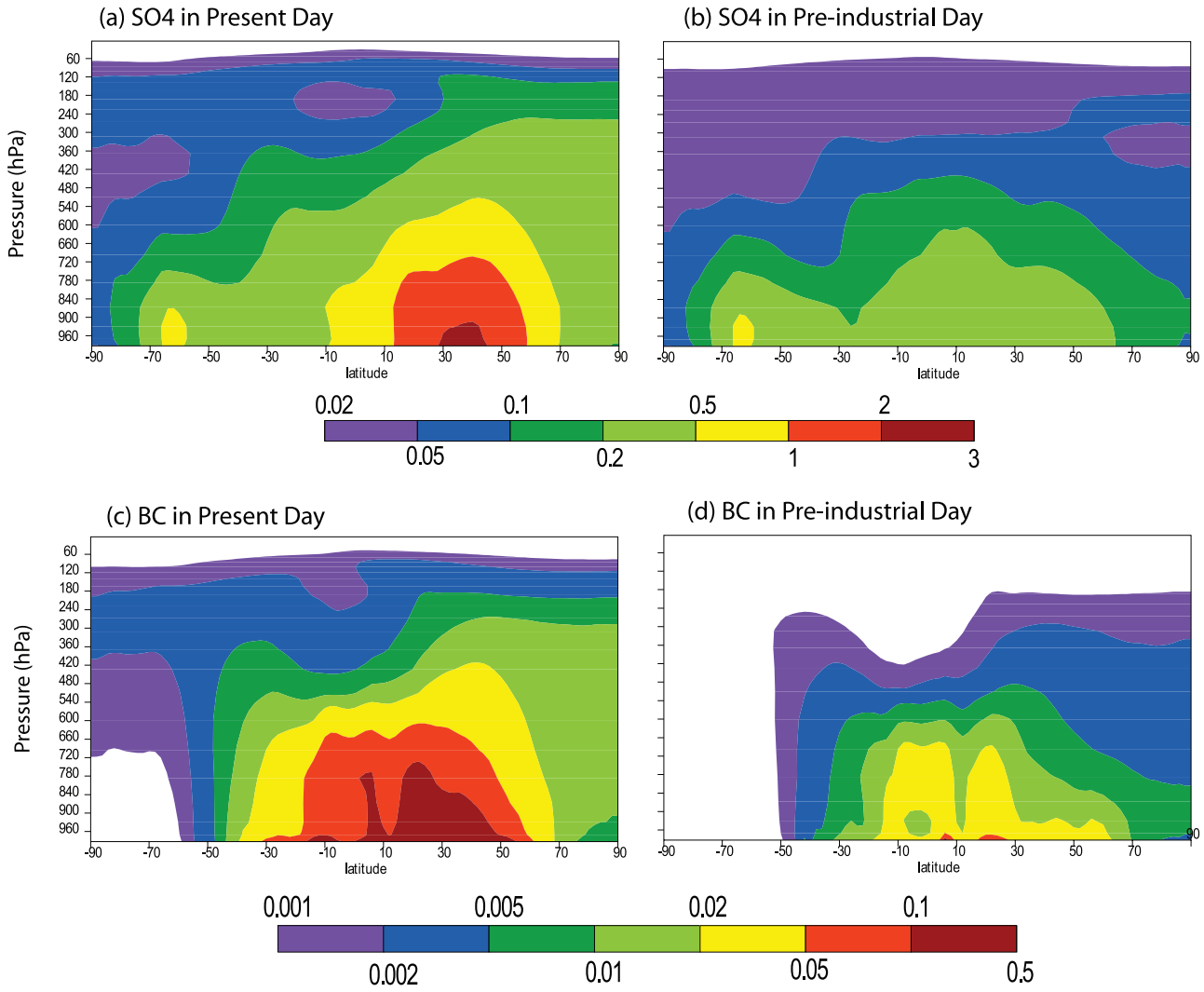


**Figure 1.** Model predicted annual average zonal mean mass concentrations ($\mu$g m$^{-3}$) of sulfate aerosol (top) and BC (bottom) for (left) present-day and (right) preindustrial day conditions. In Figure 1 and hereafter, the "white" region in Figure 1 is for values equal or less than the lowest value of color table.

from surface anthropogenic sources at 200–300 hPa typically ranges between 0.3 and 3 cm$^{-3}$ and generally exceed 1 cm$^{-3}$ in the NH midlatitude and high latitude. This result is very close to that calculated by *Hendricks et al.* [2004] who also assumed a constant number-to-mass ratio for BC from surface sources. Our calculated zonal mean aircraft BC number concentrations near 250 hPa reach 1cm$^{-3}$ in the NH midlatitude and high latitude, comparable to those from the surface anthropogenic sources. Thus aviation contributes 40–50% of the total BC number concentration in these NH regions at 200–300 hPa. *Hendricks et al.* [2004] suggested an increase in the UT/LS BC number concentration of more than 30% due to aviation in regions highly frequented by aircraft.

[27] Figure 3 shows a comparison of model predicted BC concentrations with the observational data from the works of *Blake and Kato* [1995] (BK95) and *Baumgardner et al.* [2003] (BEA03). The BK95 data set includes BC concentrations measured from aircraft in the UT/LS during different field campaigns at various locations derived from wire impactor samples which did not take into account the fractal shape of BC particles and particle bounce. *Strawa et al.* [1999] showed that the BK95 data underestimate the BC concentration by a factor of 6.15 on average. Therefore we have applied a factor of 6.15 to the BK95 data to compare with model values. Figure 3 also includes a comparison with the aircraft measurements of light absorption particles by *Baumgardner et al.* [2003] (BEA03) in the UT/LS over the North Atlantic and the Arctic Sea during the winter episode in 2003. A newly developed single particle soot photometer was used in these measurements and the uncertainty of this method is ±50%. From Figure 3, the model qualitatively captures the spatial variation of BC concentrations observed by BK95, although there is still a systematic overestimation. However, considering the large uncertainties in the BK95 data, we consider this comparison reasonable. The modeled BC concentration agrees better (within a factor of 2) with the more recent measurements by BEA03. Clearly more measurements are needed to constrain the concentrations of BC in the UT/LS.

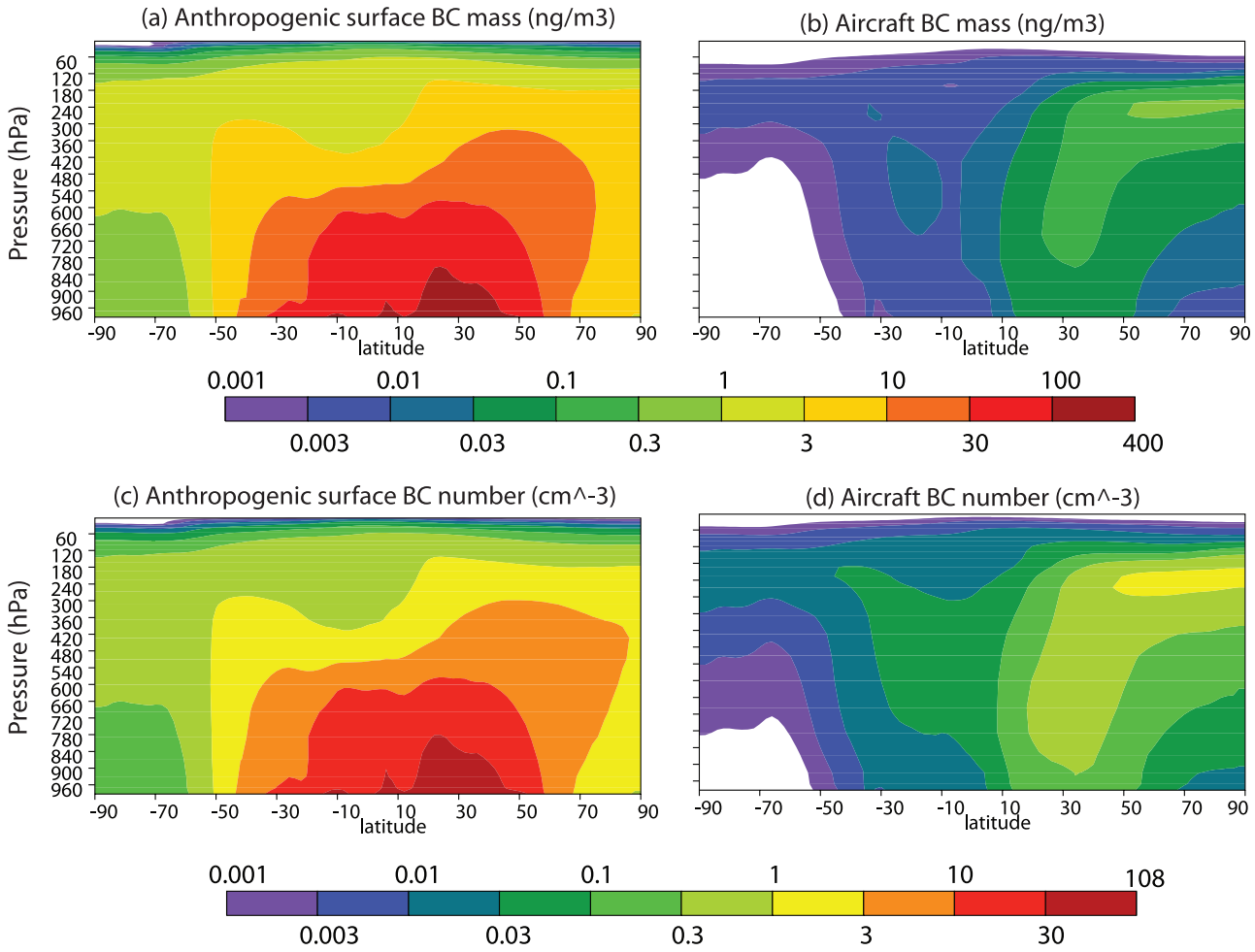


**Figure 2.** Annual average zonal mean distributions of (top) mass (ng $m^{-3}$) and (bottom) number concentrations ($cm^{-3}$) of anthropogenic BC from (left) surface and (right) from aircraft sources predicted by the coupled model.

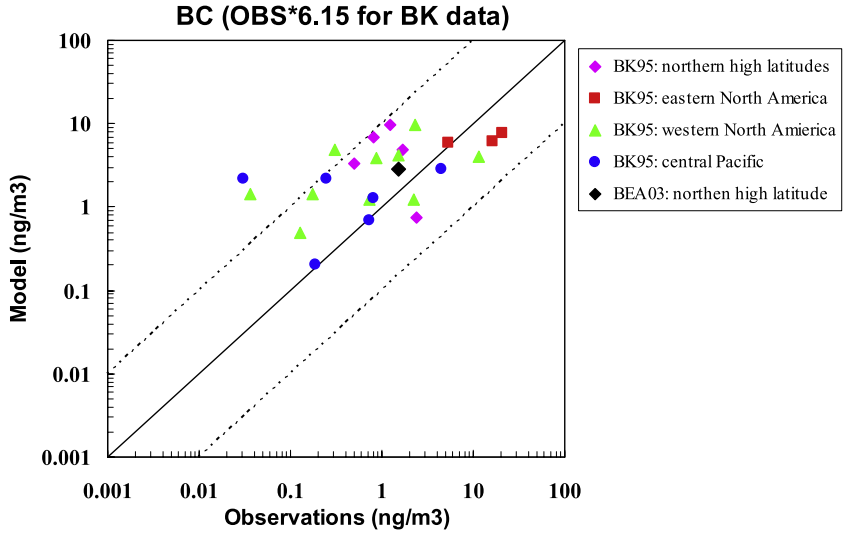


**Figure 3.** Comparison of modeled UT/LS BC concentrations with in situ aircraft measurements of BC by *Blake and Kato* [1995] (BK95) for different geographical locations and months and *Baumgardner et al.* [2003] (BEA03) for the northern high latitudes and winter season. A scaling factor of 6.15 is applied to BK95 data according to *Strawa et al.* [1999]. The solid diagonal line is 1:1, and the dashed lines are 10:1 or 1:10.

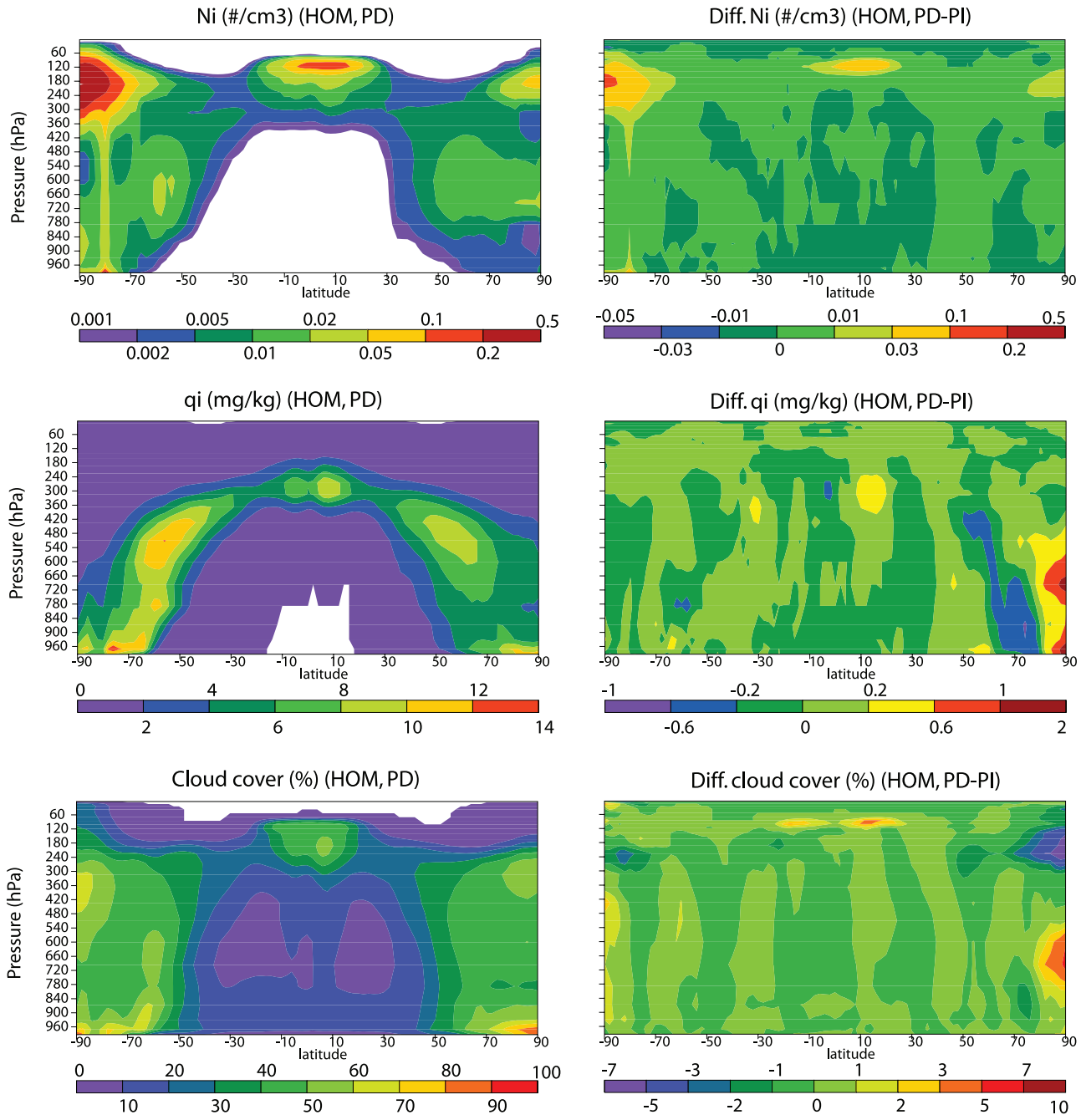


**Figure 4.** Annual average zonal mean cross sections of grid-averaged cloud ice number ($cm^{-3}$), cloud ice mass mixing ratio (mg $kg^{-3}$), and cloud cover (%) for the PD HOM simulation and the PD-PI difference.

### 3.2. Influence of Anthropogenic Sulfate Aerosol on Upper Tropospheric Cloud Ice and Water Vapor

[28] Figure 4 shows the annual average zonal mean cross sections of grid-averaged cloud ice number concentration, grid-averaged cloud ice mixing ratio and cloud cover for the HOM scenario (simulation PD) and for the difference between the PD and PI (PD-PI) simulations. Ice nucleation in the tropical upper troposphere and over polar regions produces maxima in the number concentrations of cloud ice due to the extremely low temperatures (less than −70°C) and high relative humidities, while the cloud ice mixing ratio maxima appear at lower altitudes. The simulated in-cloud ice crystal number concentrations are mostly within the range of 0.01–1 $cm^{-3}$. This represents a small number percentage (less than 1%) of the total sulfate particles which are nucleated as ice crystals (shown in Figure 5c). This percentage is higher (0.1–1%) in the tropical upper troposphere and over polar regions. *Dowling and Radke* [1990] summarized the microphysical data of cirrus from a wide number of projects before 1990 and found crystal number concentrations ranging from $10^{-7}$ to 10 $cm^{-3}$, which were widely scattered. Recent measurements of ice number con-

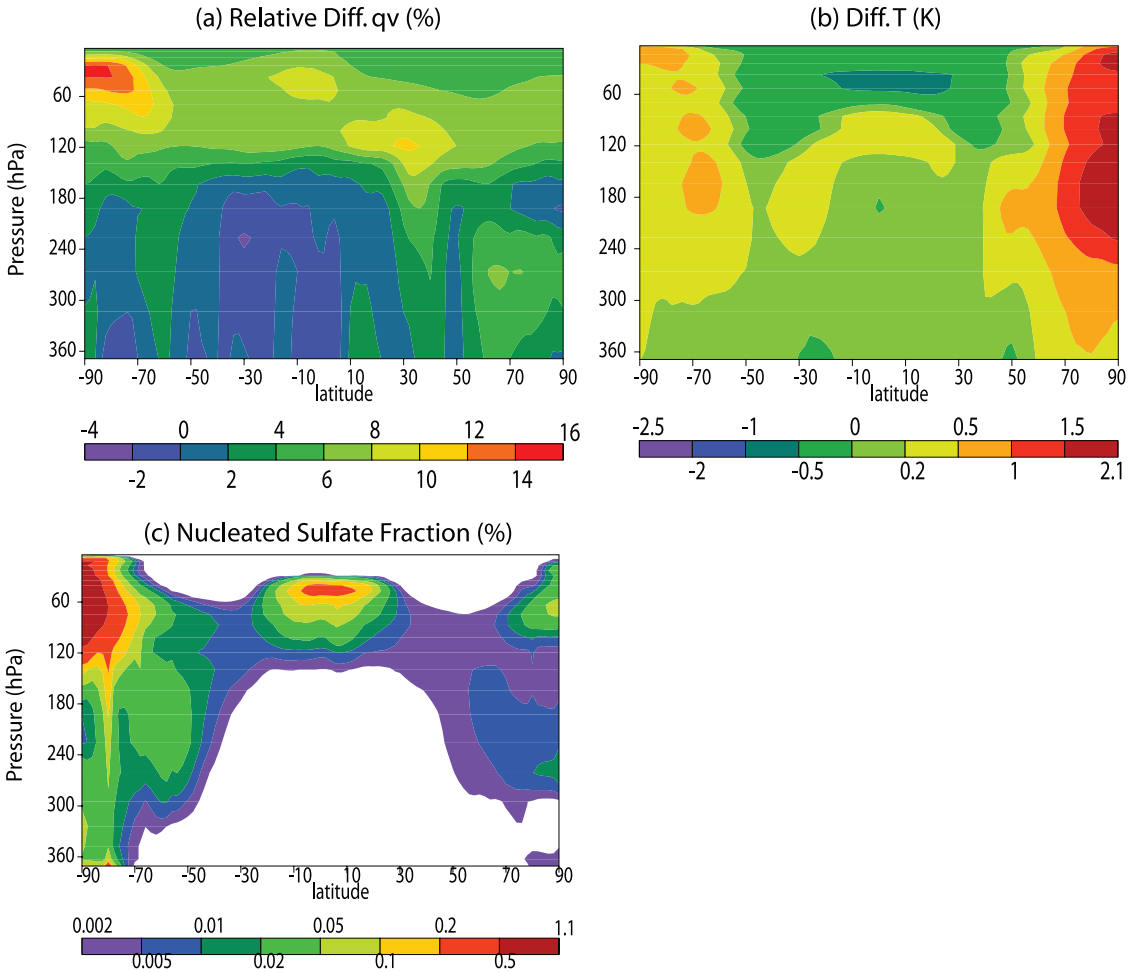


**Figure 5.** Annual zonal mean latitude versus pressure cross sections of (a) specific humidity relative difference (%), (b) temperature absolute difference (K) between the two simulations PD and PI, and (c) sulfate number fraction (%) nucleated as ice crystals for the scenario HOM.

centrations are in the range from 0.01 to 10 $cm^{-3}$. However, there are still questions about whether these high ice number concentrations are predominantly artifacts of shattering in the instrument inlets [*McFarquhar et al.*, 2007].

[29] Anthropogenic sulfate aerosol transported from mid-latitudes by the general circulation contributes to an increase in cloud ice number in the upper troposphere, most apparently in the tropical tropopause and over the Antarctic (Figure 4). The effect of increases in aerosol number concentrations on homogeneous ice nucleation is more important when temperatures are lower and updraft velocities are higher [*Kärcher and Lohmann*, 2002b; *Liu and Penner*, 2005]. The cloud ice number concentration near the tropical tropopause increases by 10% while that over the Antarctic increases by 20–30% due to a factor of 2 increase in the sulfate amount (see Figure 1). There is no significant change in cloud ice mixing ratio except below 500 hPa in the NH high latitudes where the increase over the Arctic and the reduction near 70°N can reach 10%. This strong increase over the Arctic is correlated with the increase in cloud cover there, which may be due to an amplification of climate variability near the North Pole [*Thompson and Wallace*, 2001; *Moritz et al.*, 2002]. Cloud cover near the tropical tropopause increases by 3–5%. Global total and high cloud cover increases by a very small percentage (~0.3%; Table 1). Temperatures in the upper troposphere over the Arctic increase by 1–2 K (shown in Figure 5), which is correlated with the increase in ice number concentration there (see Figure 4, top right). Increased cloud ice number near the tropical tropopause due to anthropogenic sulfate reduces the effective radius of cloud ice. Therefore ice is removed by sedimentation less readily and the air is dried less efficiently. This causes a slight warming (< 0.5 K) near the tropical tropopause due to the increased radiative heating from more cirrus clouds [*Boville et al.*, 2006] and the increased water vapor mixing ratio which is increased by ~10% (or 0.3 ppmv) in the tropical lower stratosphere. This is smaller than the increase (0.5 ppmv) between 1950 and 2000 due to anthropogenic sulfate that was calculated by *Notholt et al.* [2005]. The short-wave (SWCF) and long-wave (LWCF) cloud forcing changes by $0.30 \pm 0.17$ W $m^{-2}$ (less negative) and $0.20 \pm 0.09$ W $m^{-2}$ (more positive), respectively, between PD and PI. The reduction in the SWCF results from a decrease in cloud ice mixing ratio near 70°N as well as in the tropics as seen in Figure 4.

### 3.3. Influence of Anthropogenic Soot Aerosol on Upper Tropospheric Cloud Ice and Water Vapor

[30] Both homogeneous and heterogeneous ice nucleation and their competition are allowed in the simulation HET

**Table 1.** Global Annual Mean Changes in Liquid Water Path; Ice Water Path; Short-Wave, Long-Wave, and Net Cloud Forcing; Clear-Sky Outgoing Long-Wave Radiation; and Total and High Cloud Cover Between Present-Day and Preindustrial Simulations for HOM, HET, RHI, and NIC With Interannual Variations (Standard Deviations)[a]

| | HOM | HET | RHI | NIC |
|---|---|---|---|---|
| ΔLWP, g m$^{-2}$ | −0.02 ± 0.73 | 2.88 ± 1.14 | 0.16 ± 0.68 | 2.10 ± 0.73 |
| ΔIWP, g m$^{-2}$ | 0.02 ± 0.10 | 0.11 ± 0.14 | 0.01 ± 0.06 | 0.04 ± 0.09 |
| ΔSWCF, W m$^{-2}$ | 0.30 ± 0.17 | −1.14 ± 0.39 | 0.25 ± 0.15 | −0.72 ± 0.16 |
| ΔLWCF, W m$^{-2}$ | 0.20 ± 0.09 | 1.67 ± 0.11 | 0.45 ± 0.12 | 1.62 ± 0.08 |
| ΔCF, W m$^{-2}$ | 0.50 ± 0.11 | 0.53 ± 0.40 | 0.70 ± 0.21 | 0.91 ± 0.17 |
| ΔFLNTC, W m$^{-2}$ | −0.06 ± 0.10 | −0.46 ± 0.09 | −0.10 ± 0.12 | −0.46 ± 0.11 |
| ΔCLDTOT, % | 0.28 ± 0.30 | 1.70 ± 0.12 | 0.40 ± 0.32 | 1.72 ± 0.13 |
| ΔCLDHGH, % | 0.32 ± 0.31 | 2.51 ± 0.20 | 0.54 ± 0.22 | 2.70 ± 0.23 |

[a]LWP, liquid water path; IWP, ice water path; SWCF, short-wave cloud forcing; LWCF, long-wave cloud forcing; CF, net cloud forcing; FLNTC, clear-sky outgoing long-wave radiation; CLDTOT, total cloud cover; CLDHGH, high cloud cover.

with a threshold $RH_i$ for heterogeneous ice nucleation of 120–130% for soot particles [*Liu and Penner*, 2005]. It is noted that the role of soot particles in ice nucleation is still unknown [*Kärcher et al.*, 2007] and the HET scenario would be regarded as an upper limit to the possible effects of soot particles on cirrus clouds and water vapor, since heterogeneous soot nucleation may take place at a higher $RH_i$. Figure 6 shows the annual average zonal mean changes in ice crystal number concentration, cloud ice mixing ratio and cloud cover between PD and PI for the HET scenario. Cloud ice number increases by a factor of 2 over polar regions due to the nucleation of anthropogenic soot transported from the midlatitudes (see Figure 1) and due to the extremely low temperatures over the poles. There is a general increase in cloud ice mixing ratio in the upper troposphere, especially in the tropics and extratropics where increases can reach 10%. This is consistent with the slower sedimentation of cloud ice with smaller sizes. Cloud ice

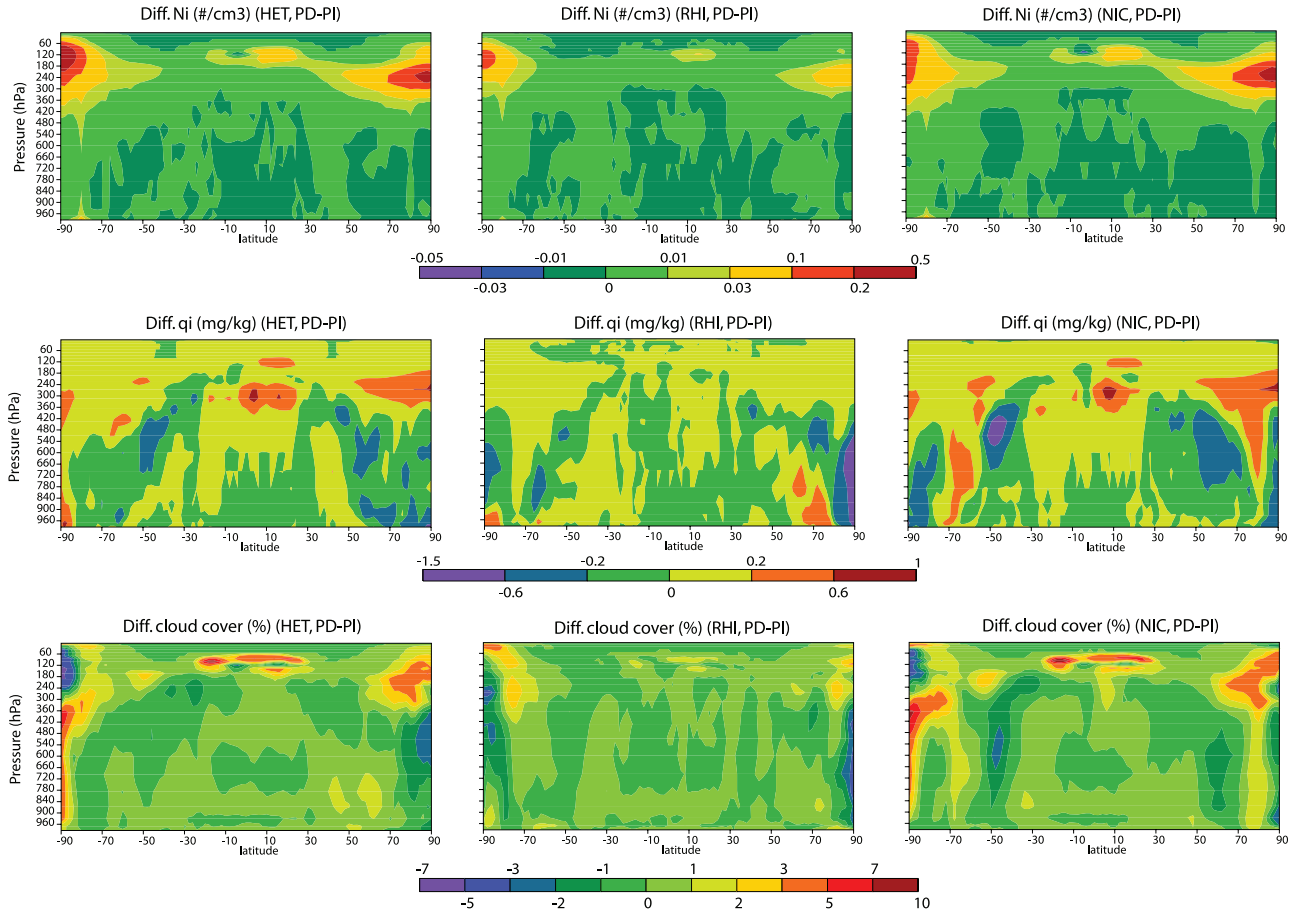


**Figure 6.** Annual average zonal mean cross sections of (top) cloud ice number difference (cm$^{-3}$), (middle) cloud ice mass mixing ratio difference (mg kg$^{-3}$), and (bottom) cloud cover difference (%) between PD and PI simulations for HET, RHI, and NIC.

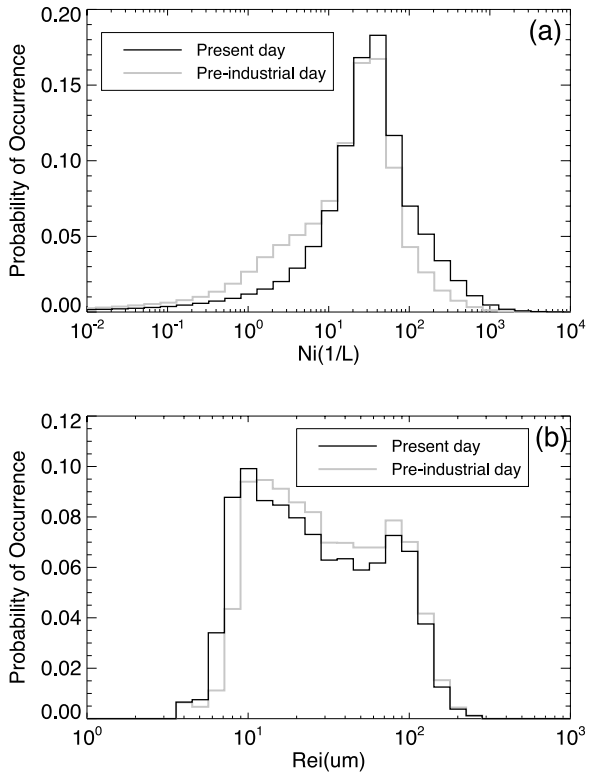


**Figure 7.** Frequency distribution of (a) cloud ice number concentrations ($L^{-1}$) and (b) ice effective radii ($\mu$m) in the upper troposphere with temperature less than $-35$°C and within 20°S and 20°N in the PD and PI simulations for the HET scenario.

mixing ratio is reduced beneath these regions. Cloud cover is also enhanced in most of the upper troposphere with global high cloud cover increased by 2.5% (see Table 1). SWCF and LWCF change by $-1.14 \pm 0.39$ (cooling) and $1.67 \pm 0.11$ W m$^{-2}$ (warming), respectively, between the PD and PI simulations. Comparing the HET with the HOM scenario (with only the effect of sulfate), anthropogenic soot aerosol (from surface and aircraft sources) increases both the SWCF (more negative) and the LWCF (more positive) by approximately the same amount ($\sim$1.5 W m$^{-2}$). The net cloud forcing (CF) change is $0.53 \pm 0.40$ W m$^{-2}$ (warming) for the HET scenario. It is noted that these forcing changes include the climate feedbacks between cloud ice effective sizes (and thus cirrus cloud optical properties), ice gravitational settling, and changes in cloud ice mixing ratio, water vapor, and cloud cover. The above radiative forcing does not include changes in mixed-phase clouds associated with the Bergeron-Findeisen process since we do not consider changes in ice number concentrations in mixed-phase clouds due to anthropogenic aerosols (sulfate and soot).

[31] Figure 7 shows the frequency distribution of cloud ice number concentrations and ice effective radii in the upper troposphere with temperatures less than $-35$°C and within 20°S and 20°N in the PD and PI simulations for HET. Clearly, cloud ice number concentrations (grid averaged) increase and the frequency distribution moves toward larger number concentrations in the PD simulation. There are two peaks in the frequency distribution of cloud ice effective radius. The peak at smaller radius is associated with cirrus clouds formed near the tropical tropopause with higher ice number concentrations (see Figure 6, top), and peak at the larger radius occurs at lower altitudes in appropriately the same locations as the maximum cloud ice mass mixing ratio (Figure 4). The frequency distribution associated with the lower radius is shifted toward a smaller radius (by $\sim$15%) due to anthropogenic aerosols.

[32] Figure 8 shows the changes in water vapor mixing ratio and air temperature between the PD and PI simulations for the HET scenario. The zonal mean water vapor mixing ratio in the lower stratosphere increases by 20–45% between the preindustrial and present-day simulations. This results mainly from the higher temperatures at the tropical tropopause which increases the water vapor saturation pressure at the cold trap. Temperatures near the tropopause are warmer by 1–2 K due to the increased radiative heating by ice clouds with their larger numbers of smaller ice particles (Figure 7).

### 3.4. Sensitivity Tests for Heterogeneous Ice Nucleation

[33] There are still large uncertainties associated with the importance of heterogeneous nucleation on soot in cirrus cloud formation due to a lack of information on the nucleation properties of soot [*Kärcher et al.*, 2007]. Therefore we conducted two sensitivity tests on ice nucleation for the pair of PD and PI simulations: in the first test (RHI) the threshold $RH_i$ for heterogeneous ice nucleation was increased from the control run (HET; 120–130% as a weak function of temperature) to 140% to represent less efficient ice nucleation on soot. In the second test (NIC) we used the *Gierens* [2003] critical IN number concentration (as a function of temperature and updraft velocity) instead of that from the work of *Liu and Penner* [2005]. To examine the possible impact of higher $RH_i$ associated with subgrid scale variability in updrafts, we performed a third sensitivity test by adding 20% to the calculated $RH_i$ in determining the number of ice crystals nucleated.

[34] With the higher threshold $RH_i$ of 140% for soot nucleation, the changes in the cloud ice number between the PD and PI simulations are substantially reduced over the polar regions and near the tropical tropopause (Figure 6). The same is true for the cloud ice mixing ratio and cloud fraction in the upper tropophere except over the poles. Global total and high cloud cover increase by 0.4 and 0.5%, respectively, between the PD and PI (Table 1). Water vapor changes by less than 10% in the lower stratosphere, and temperatures by less than 0.5 K near the tropical tropopause (Figure 8). The global SWCF and LWCF change due to anthropogenic sulfate and BC is $0.25 \pm 0.15$ (warming) and $0.45 \pm 0.12$ W m$^{-2}$ (warming), respectively, between the PD and PI simulations. Soot particles alone contribute to the LWCF increase by 0.25 W m$^{-2}$, comparing the LWCF change in the RHI scenario to that in the HOM scenario. The change in the global mean SWCF between the HOM and RHI simulations is similar (Table 1).

[35] With a different formulation for the critical IN number concentration [*Gierens*, 2003] (simulation NIC), the pattern in the changes of cloud ice number concentration and mixing ratio, cloud cover, water vapor and temperatures between the PD and PI simulations is very similar to those from the HET simulations (see Figures 6 and 8). The change

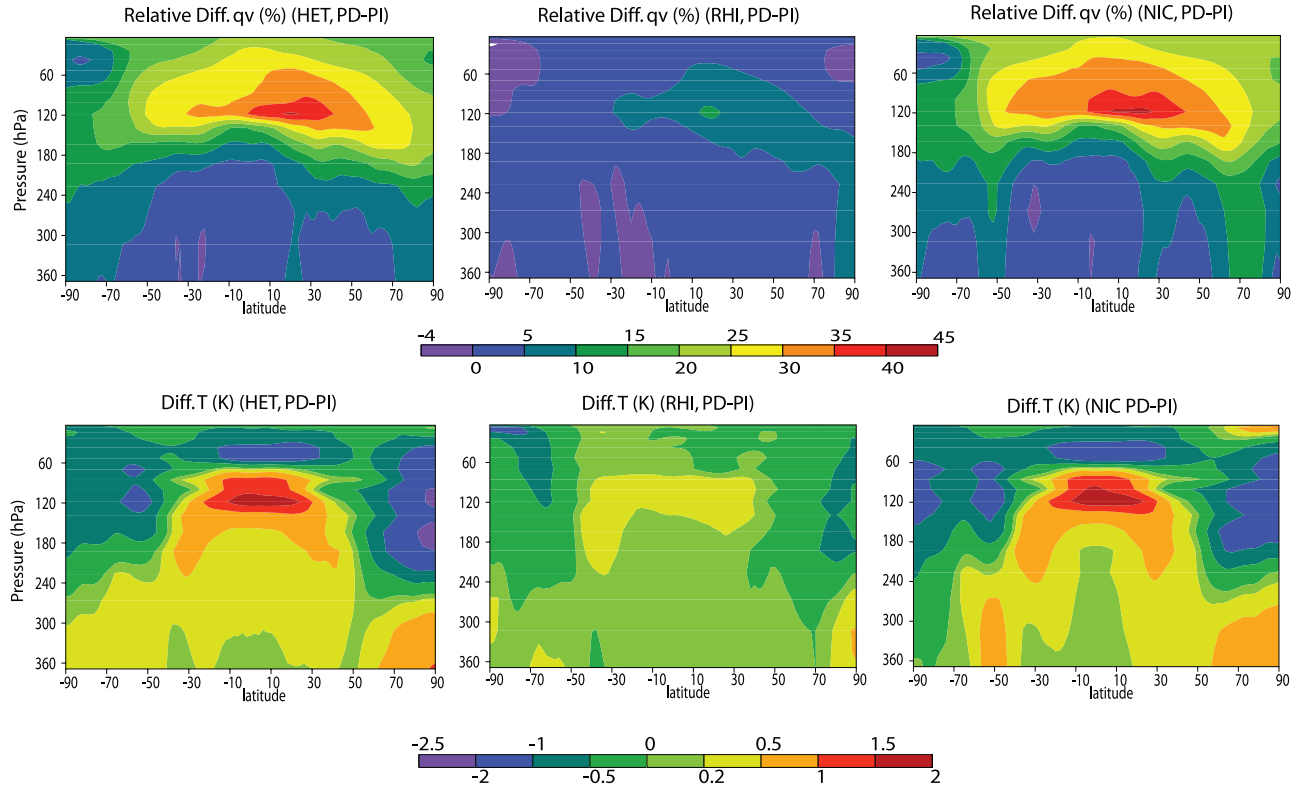


**Figure 8.** Annual average zonal mean cross sections of (top) specific humidity relative difference (%) and (bottom) temperature absolute difference (K) between PD and PI simulations for HET, RHI, and NIC.

in cloud ice number concentration is reduced over the Antarctic. The global mean changes are very close between the HET and NIC scenarios except that the magnitude in the SWCF change is reduced from $-1.14 \pm 0.39$ to $-0.72 \pm 0.16$ W m$^{-2}$ (see Table 1).

[36] When the $RH_i$ is increased by 20% in the calculation of nucleation, ice nucleation occurs much more frequently compared to the HET scenario, and zonal mean cloud ice number concentrations increase significantly. Global mean high-cloud fraction increases 4.5%. SWCF and LWCF increase by $\sim$11 W m$^{-2}$ for the PD simulation although the net CF change is negligible. Changes in cloud properties (cloud cover, cloud ice mixing ratio and number), and water vapor and temperature in UT/LS between the PD and PI simulations are more dramatic than in the HET scenario. Clearly a better treatment of the subgrid scale variability of $RH_i$ is needed which could link not only to ice nucleation but to other aspects of cloud macrophysics (e.g., cloud cover) and microphysics.

## 4. Indirect Forcing by Anthropogenic Sulfate and Soot on Cirrus Clouds

[37] The previous section shows the anthropogenic aerosol influence on cirrus clouds by comparing the PD and PI simulations. The change in clouds is due to the combined effects of different aerosol components. In this section the indirect forcing of individual aerosol components (sulfate, surface soot, and aircraft soot) is calculated and given in Table 2. For these calculations, the present-day simulations are repeated, but with the present-day industrial emissions for sulfate (simulation PD-so4), for surface soot (simulation PD-sfcsoot), and for aircraft soot emission (simulation PD-airsoot) removed. The cloud forcing differences between the PD simulations and these simulations are calculated for the forcing of the individual aerosol components. The above simulations are performed for both HET (with lower heterogeneous $RH_i$ threshold) and RHI scenarios (with higher heterogeneous $RH_i$ threshold).

[38] From Table 2, the changes in the SWCF and LWCF due to soot from surface sources are $-1.13 \pm 0.26$ and $1.35 \pm 0.15$ W m$^{-2}$, respectively if surface soot can act as an efficient IN in the HET scenario, and are reduced significantly to $0.22 \pm 0.42$ and $0.17 \pm 0.18$ W m$^{-2}$, respectively, if surface soot is less efficient as an IN in the RHI scenario. The change in the LWCF due to soot from aviation (aircraft soot) is $0.12 \pm 0.17$ and $0.06 \pm 0.16$ W m$^{-2}$, respectively, for the HET and RHI scenarios. The sum of the two LWCF changes due to surface soot and aircraft soot is 1.47 and 0.23 W m$^{-2}$, respectively, for the HET and RHI simulations, which are almost the same as those calculated for the total anthropogenic soot aerosol effects (including surface and aircraft soot) on the LWCF in section 3 (i.e. 1.47 W m$^{-2}$ for HET and 0.25 W m$^{-2}$ for RHI from the difference between the HET and RHI simulations and the HOM simulation in Table 1). The SWCF changes are positive (warming) in the RHI scenario (related to the reduction in the cloud ice mixing ratio). However, the interannual variability is comparable or even larger. The LWCF change due to anthropogenic sulfate is smaller ($0.08 \pm 0.15$ W m$^{-2}$ for HET and $0.01 \pm 0.14$ W m$^{-2}$ for RHI) than that derived for the HOM scenario ($0.20 \pm$

**Table 2.** Global Mean SWCF, LWCF, and Net Cloud Forcing Changes and Interannual Variability (Standard Deviation) Due to Anthropogenic Aerosols (Surface Soot, Aircraft Soot, and Sulfate)[a]

| | | Surface Soot | Aircraft Soot | Sulfate | All Aerosols |
|---|---|---|---|---|---|
| ΔSWCF, W m$^{-2}$ | HET | −1.13 ± 0.26 | −0.23 ± 0.27 | −0.07 ± 0.27 | −1.14 ± 0.39 |
| | RHI | 0.22 ± 0.42 | 0.20 ± 0.25 | 0.31 ± 0.27 | 0.25 ± 0.15 |
| ΔLWCF, W m$^{-2}$ | HET | 1.35 ± 0.15 | 0.12 ± 0.17 | 0.08 ± 0.15 | 1.67 ± 0.11 |
| | RHI | 0.17 ± 0.18 | 0.06 ± 0.16 | 0.01 ± 0.14 | 0.45 ± 0.12 |
| ΔCF, W m$^{-2}$ | HET | 0.22 ± 0.24 | −0.11 ± 0.27 | 0.01 ± 0.36 | 0.53 ± 0.40 |
| | RHI | 0.39 ± 0.35 | 0.26 ± 0.14 | 0.31 ± 0.26 | 0.70 ± 0.21 |

[a]Values for both HET and RHI scenarios are included.

0.09 W m$^{-2}$) because the change in ice number concentration due to sulfate in the HET and RHI scenarios is smaller than in the HOM scenario. The cloud forcing changes due to all anthropogenic aerosols listed in Table 2 are those presented in section 3.

[39] Figure 9 shows cloud ice number changes due to soot from surface and from aircraft sources, which are calculated from the differences between the PD and PD-sfcsoot simulations and between the PD and PD-airsoot simulations, respectively. Surface soot increases cloud ice number by 30–50% in the extratropics in both hemispheres and near the tropical tropopause in the HET scenario assuming soot is an efficient IN (there is a reduction in ice number in some regions of the tropics due to the competition between soot and sulfate nucleation). Soot from aircraft sources also increases the cloud ice number in both hemispheres in the polar regions and in the NH extratropics. In the RHI scenario, where soot is a less efficient IN, surface and aircraft soot only increase ice number significantly in the NH extratropics with an ∼20% reduction in the tropics associated with surface soot.

[40] Figure 10 shows the change in the net cloud forcing resulting from the perturbation by anthropogenic soot (both from surface and aircraft sources) and by all anthropogenic aeorosls (sulfate and soot) for the scenario HET between the PD and PI simulations. Regions where the forcing change is statistically significant using a Student's *t* test at the 90% confidence interval are cross hatched (we used the 90% level because of the small sample number which is 5). In contrast to the indirect effect of anthropogenic aerosol on

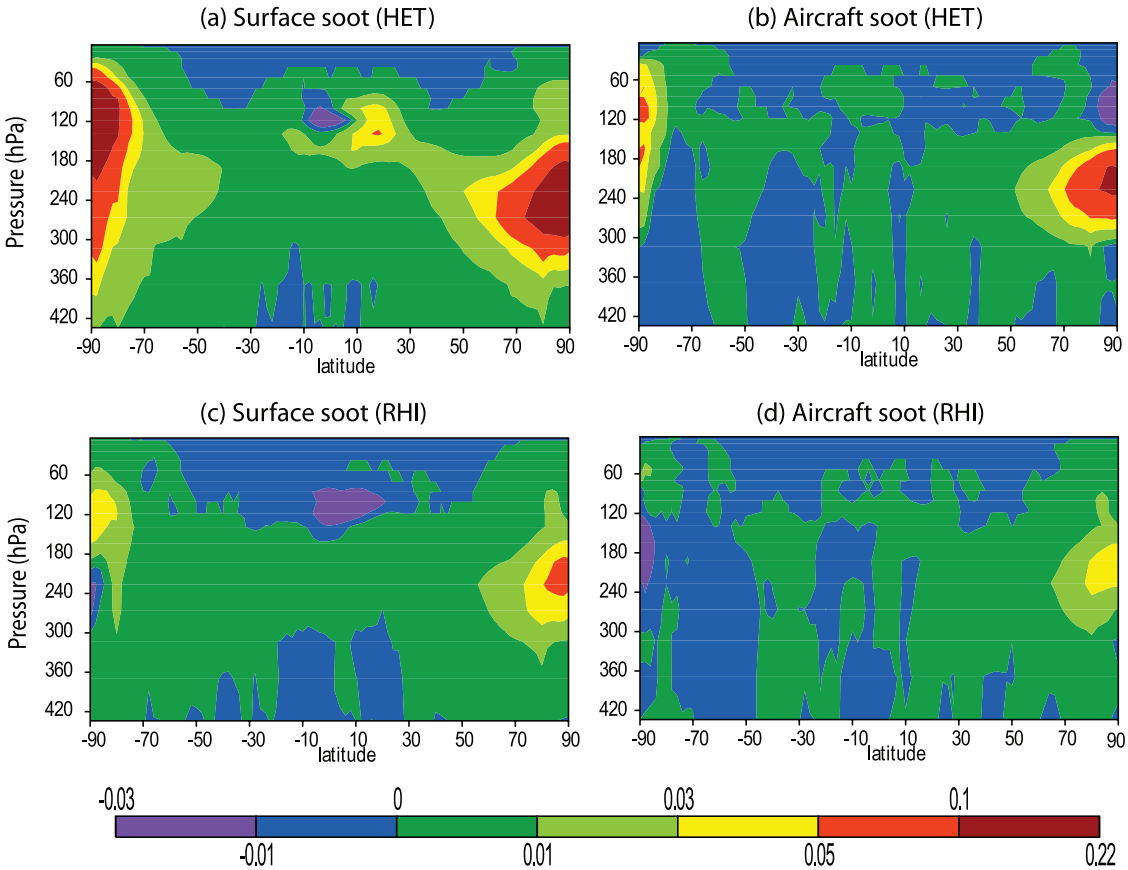


**Figure 9.** Annual average zonal mean cross sections of cloud ice number differences (cm$^{-3}$) resulting from (left) anthropogenic surface soot and (right) aircraft soot for the (top) HET and (bottom) RHI scenarios.

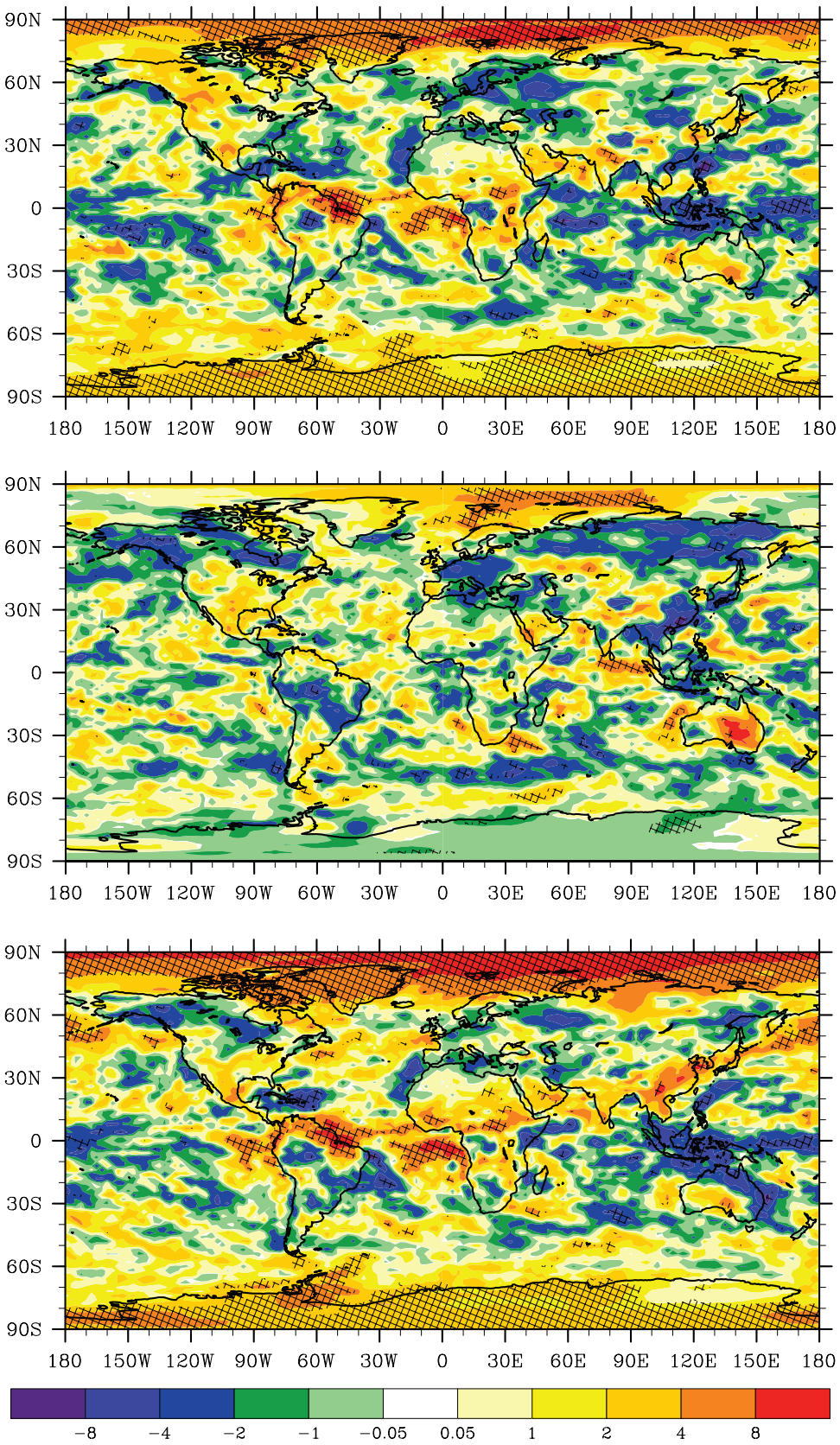


**Figure 10.** Annual net cloud forcing change (in unit of W $m^{-2}$) resulting from perturbation by anthropogenic soot from surface (top) and from aircraft sources (middle) and by all anthropogenic aerosols (bottom) for scenario HET. The cross-hatched areas depict the regions where forcing change is statistically significant with a Student's *t* test.

liquid-water clouds where the zonal mean flux changes exceeds the standard deviations in the NH low and midlatitudes [e.g., *Ming et al.*, 2007], the aerosol soot perturbation on ice clouds from the HET scenario is only statistically significant at high latitudes in the case of surface soot and in the NH high latitudes of Europe for the aircraft soot simulation. Regions with a significant change are generally associated with positive forcing. The overall forcing is stronger and areas where forcing change is statistically significant larger in the Arctic and in the tropics than the forcing due to surface soot alone (Figure 10, compare top and bottom). In the RHI scenario (Figure 11) the net cloud forcing change due to the soot effect and due to all anthropogenic aerosols is smaller at high latitudes. The net cloud forcing change is significant in the SH high latitudes, part of Greenland and some regions of the subtropics where there is a radiative warming by surface soot. The net forcing change due to aircraft soot is generally insignificant in the RHI scenario.

## 5. Discussion

[41] We compare our results with simulations from *Penner et al.* [2008] who used an offline version of the aerosol and meteorological fields from the IMPACT aerosol model and CAM3 to calculate cloud ice number concentrations and the resulting cloud forcing changes due to anthropogenic aerosols. Both the mass-only version and the three-mode version of the IMPACT aerosol model were used. Two ice nucleation parameterizations were used: *Liu and Penner* [2005] and *Kärcher et al.* [2006]. When applying *Kärcher et al.*'s [2006] parameterization, *Penner et al.* [2008] ran a cloud parcel model starting with 100% $RH_i$ within cloud and tracked the rising parcel for 30 minutes (or until a maximum in the calculated $RH_i$ is reached, whichever is first) to determine ice nucleation. When applying the *Liu and Penner* [2005] parameterization, the threshold $RH_i$ for both homogeneous and heterogeneous ice nucleation (e.g., equation (2)) was abandoned and the threshold soot number and temperature were used to differentiate between homogeneous and heterogeneous nucleation (i.e., equation (3)). In the mass-only simulations with the *Kärcher et al.* [2006] treatment as well as the three-mode simulations with both the *Kärcher et al.* [2006] and *Liu and Penner* [2005] treatments homogeneous nucleation dominates in the PI simulation and cloud ice number concentration is reduced in the NH above 200 hPa due to anthropogenic surface soot. The global annual average LWCF and net cloud forcing changes between the PD and PI simulations are negative. In the mass-only simulation with the *Liu and Penner* [2005] parameterization, the global annual averaged LWCF and net cloud forcing changes between the PD and PI simulations are positive, but significantly smaller than those found here. This is because homogeneous nucleation dominates to a greater extent than that calculated here, where the grid average $RH_i$ is used with the *Liu and Penner* [2005] parameterization. We note that the CAM simulations reported here significantly underestimate the occurrence of high supersaturations compared with the MOZAIC observations (LIU07). Another important difference between the current study and that of *Penner et al.* [2008] is that this study allows cloud feedbacks which cause an increase in high-cloud fraction due to anthropogenic aerosols (see Figure 6 and Table 1). Since long-wave cloud forcing is dominant for cirrus clouds, a positive net cloud forcing in this study is also associated with the increased cloud amount in addition to changes in cloud ice number and sizes due to anthropogenic aerosols. Nevertheless, both studies suggest the importance of understanding the ice nucleation properties of soot in order to understand their global climate impact.

[42] In this study, the effect of soot emitted from aircraft on cirrus clouds and their radiative forcing is calculated. It is found that aircraft soot can increase ice number concentrations by 30% in the NH extratropics (north of 50°N) when it is an efficient IN (HET scenario). This is consistent with the 10–60% increase in cloud ice number concentrations from the work of *Hendricks et al.* [2005], when they assumed that all aircraft soot particles can nucleate ice. Our calculated LWCF perturbation due to aircraft soot is $0.12 \pm 0.17$ W m$^{-2}$. However, the cloud ice number concentration change is less than 10% in the NH extratropics and change in the LWCF is only $0.06 \pm 0.16$ W m$^{-2}$ when soot requires a higher threshold $RH_i$ for nucleation (140%). It is noted that in this study we are using a different aircraft emission inventory than that by *Hendricks et al.* [2005]. Our total emission is 0.0056 Tg C a$^{-1}$ for the year 1992 compared to 0.0047 Tg C a$^{-1}$ from the work of *Hendricks et al.* [2004]. In addition, the emissions used by *Hendricks et al.* [2004] had larger emission indices (defined as the amount of soot released per burnt mass of fuel) for soot emissions rates close to the ground and a lower emission index in the midtroposphere and upper troposphere than that for our inventory. Thus a lower aircraft soot impact on upper tropopheric clouds may be expected had we used the *Hendricks et al.*'s [2004] emissions.

[43] This study shows the large sensitivity of aerosol radiative forcing in cirrus clouds to the ice nucleation efficiency of soot particles. As indicated by *Mitchell et al.* [2008], the sensitivity of ice fall speed to ice particle size may be underestimated in CAM3. Changes in ice particle size and fall speed were shown to have large impacts on cirrus clouds through climate feedbacks to cirrus clouds [*Mitchell et al.*, 2008; *Sanderson et al.*, 2008]. Thus the radiative forcing of anthropogenic aerosols on cirrus clouds and the uncertainty associated with the forcing can be larger than that suggested in this study. This points out the importance of a better treatment of the ice particle size distribution, shape and fall speed in climate models.

[44] Our treatment of cloud condensates is based on the double-moment method, i.e., the mass and number of cloud condensates are predicted. Ice nucleation is one of the terms in the prognostic equations and is derived from a detailed cloud parcel model simulation with a size-resolved treatment for both the aerosol and the ice nucleation processes. We note that if a discrete size-resolved treatment of aerosols and cloud condensates were used in this study, the radiative forcing might change. However, the purpose of this study is to demonstrate the possible magnitude of cloud forcing and the large uncertainty in the radiative forcing associated with the ice nucleation treatment. Certainly different cloud microphysics treatments or climate models may lead to changes in the forcing so that it would be useful to repeat this study using other climate models.

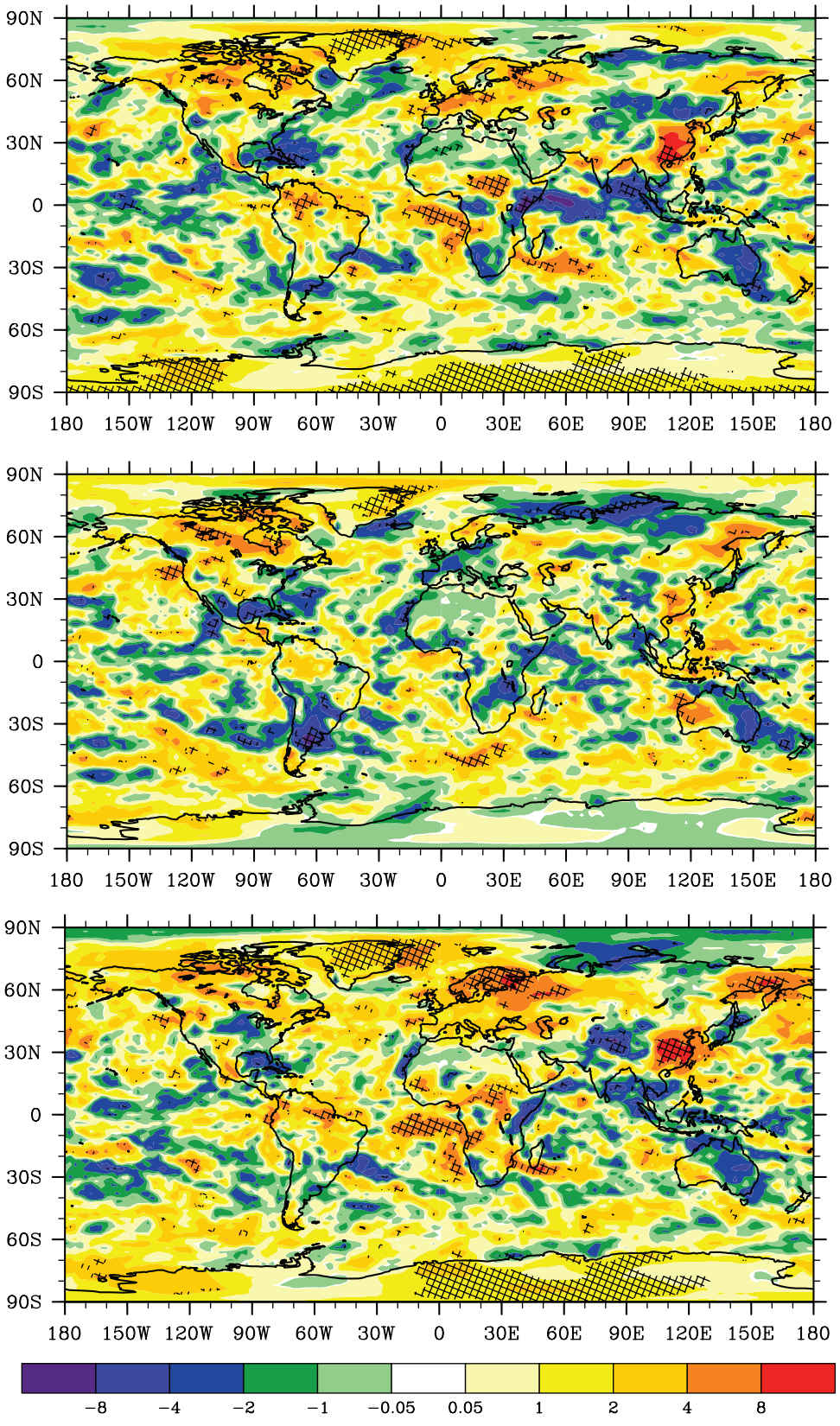


**Figure 11.** Same as Figure 10, but for scenario RHI.

[45] In this study, climatological SSTs were used in our simulations. Thus the temperature changes to the oceans due to changes in clouds are not treated. Changes to SSTs would affect both the water vapor and UTLS temperature change predictions. The main focus of this study is not on climate feedbacks, but rather on the cloud radiative forcing caused by aerosol-cirrus interactions, and we also document the large sensitivity of water vapor and changes in the UTLS temperature to ice nucleation. It is very likely that allowing changes to the SSTs will result in larger water vapor and temperature changes through cloud feedbacks. Thus a more accurate prediction of the change in water vapor and UTLS temperature will require using a coupled atmosphere and ocean model, e.g., CCSM [*Collins et al.*, 2006].

## 6. Summary and Conclusions

[46] In this study, the influence of anthropogenic aerosols (sulfate and soot) on upper tropospheric cirrus clouds and water vapor was examined using the modified NCAR CAM3 climate model which accounts for ice supersaturation and ice nucleation on aerosols coupled to a global aerosol model (IMPACT). Two simulation scenarios are considered for pairs of PD and PI simulations with different anthropogenic aerosol emissions. In HOM, it is assumed that homogeneous ice nucleation on sulfate dominates ice nucleation in upper tropospheric cirrus clouds, and in HET, both the homogeneous and heterogeneous ice nucleation are allowed to take place and compete with each other. Two additional sensitivity tests were performed to study the effect of the threshold $RH_i$ for heterogeneous ice nucleation and the critical IN number concentration that determines the transition from homogeneous nucleation to heterogeneous nucleation.

[47] In the HOM scenario, anthropogenic sulfate results in an increase in cloud ice number by 20–30% over the Antarctic and by 10% over the tropical upper troposphere between the PD and PI simulations. Cloud cover near the tropical tropopause increases by 3–5%, and temperature increases by less than 0.5 K. Lower stratosphere water vapor increases by ~10% (or 0.3 ppmv) which is a result of the warming near the tropical tropopause associated with the higher cloud ice number concentrations there. This result is smaller than the increase (0.5 ppmv) between 1950 and 2000 due to anthropogenic sulfate calculated by *Notholt et al.* [2005]. The change in the SWCF and LWCF is $0.30 \pm 0.17$ W m$^{-2}$ (less negative) and $0.20 \pm 0.09$ W m$^{-2}$ (more positive), respectively.

[48] In the HET scenario with competition between homogeneous and heterogeneous ice nucleation and with a threshold $RH_i$ of 120–130% for heterogeneous ice nucleation on soot, cloud ice number increases by a factor of 2 over the polar regions between the PD and PI simulations due to efficient nucleation on anthropogenic soot transported from midlatitudes. The general increase in ice number from PI to PD due to anthropogenic soot implies that ice nucleation is dominated by heterogeneous nucleation in both PD and PI simulations in the HET scenario when soot is an efficient IN. Cloud ice mass mixing ratio increases by 10% in the tropical and extratropical upper troposphere and decreases below these regions. Global high cloud cover is enhanced by 2.5%. The change in the SWCF and LWCF is $-1.14 \pm 0.39$ (cooling) and $1.67 \pm 0.11$ W m$^{-2}$ (warming), respectively. Compared with the HOM simulation, anthropogenic soot increases the change in the LWCF by 1.5 W m$^{-2}$ (with 1.35 W m$^{-2}$ from surface soot and 0.12 W m$^{-2}$ from aircraft soot). The tropical tropopause temperature increases by 1–2 K and lower stratospheric water vapor increases by 20–45%.

[49] The influence of soot is significantly reduced when a higher threshold $RH_i$ for ice nucleation (140%) is used. Global high cloud cover increases by 0.5% between the PD and PI simulations (Table 1). Water vapor increases by less than 10% in the lower stratosphere, and the temperature increases by less than 0.5 K near the tropical tropopause. The change in the global average SWCF and LWCF due to anthropogenic aerosols is $0.25 \pm 0.15$ (warming) and $0.45 \pm 0.12$ W m$^{-2}$ (warming), respectively, between the PD and PI simulations. Comparing these changes with those from the HOM scenario with only the sulfate effect, soot particles contribute to an increase in LWCF by 0.23 W m$^{-2}$ (with 0.17 W m$^{-2}$ from surface soot and 0.06 W m$^{-2}$ from aircraft soot). The change in the global mean SWCF is similar between the HOM and RHI simulations. Our results reinforce the importance of understanding of the ice nucleation efficiency by soot particles [*Kärcher et al.*, 2007] from the point view of their influence on cirrus clouds and UT/LS water vapor. We do not find a high sensitivity to the critical IN number concentration for the transition from homogeneous to heterogeneous ice nucleation. This is probably due to the fact that the two formulations used for determining the critical IN number [*Liu and Penner*, 2005; *Gierens*, 2003] differ only when updraft velocity is less than 0.1 m s$^{-1}$ and average ice number concentrations are mainly determined by the higher updrafts when integrated over the Gaussian distribution of updraft velocity.

[50] We note that we have not differentiated between the ice nucleation efficiency of surface and aircraft soot. Soot particles in the atmosphere with different sources (biomass burning, different kinds of fossil fuel combustion, and aircraft) can have different sizes, morphologies and possibly also different ice nucleation properties. However, there is not enough known about the nucleation properties of these different soot particles to resolve these differences.

[51] **Acknowledgments.** The authors acknowledge the support from the National Science Foundation as well as the NASA IDS program under grants ATM 0333016 and NNG04GC01G, respectively. Partial support from the Department of Energy (DOE) Environmental Science Division Atmospheric Radiation Measurement (ARM) program is also gratefully acknowledged. X. L. thanks Yi Wang with the help of making some plots. The Pacific Northwest National Laboratory is operated for the DOE by Battelle Memorial Institute under contract DE-AC06-76RLO 1830.

## References

Andres, R. J., and A. D. Kasgnoc (1998), A time-averaged inventory of subaerial volcanic sulfur emissions, *J. Geophys. Res.*, *103*, 25,251–25,261.

Baughcum, S. L., T. G. Tritz, S. C. Henderson, and D. C. Pickett (1996), Scheduled civil aircraft emission inventories for 1992: Database development and analysis, *NASA Contr. Rep. CR-4700*, p. 205, National Aeronautics and Space Administration, Hampton, VA, USA.

Baumgardner, D., G. Kok, G. Raga, G. Diskin, and G. Sachse (2003), Black carbon measurements in the arctic UT/LS, Proceedings of the European Aerosol Conference 2003, *J. Aerosol Sci.*, 979–980.

Blake, D. F., and K. Kato (1995), Latitudinal distribution of black carbon soot in the upper troposphere and lower stratosphere, *J. Geophys. Res.*, *100*, 7195–7202.

Boville, B. A., P. J. Rasch, J. J. Hack, and J. R. McCaa (2006), Representation of clouds and precipitation processes in the Community Atmosphere Model version 3 (CAM3), *J. Clim.*, *19*, 2184–2198.

Chen, Y., S. M. Kreidenweis, L. M. McInnes, D. C. Rogers, and P. J. DeMott (1998), Single particles analyses of ice nucleating aerosols in the upper troposphere and lower stratosphere, *Geophys. Res. Lett.*, *25*, 1391–1394.

Collins, W. D., et al. (2006), The Community Climate System Model version 3 (CCSM3), *J. Clim.*, *19*, 2122–2143.

Cziczo, D. J., D. M. Murphy, P. K. Hudson, and D. S. Thomson (2004), Single particle measurements of the chemical composition of cirrus ice residue during CRYSTAL-FACE, *J. Geophys. Res.*, *109*, D04201, doi:10.1029/2003JD004032.

Danilin, M. Y., et al. (1998), Aviation fuel tracer simulation: Model intercomparison and implications, *Geophys. Res. Lett.*, *25*, 3947–3950.

DeMott, P. J. (1990), An exploratory study of ice nucleation by soot aerosols, *J. Appl. Meteorol.*, *29*, 1072–1079.

DeMott, P. J., D. C. Rogers, and S. M. Kreidenweis (1997), The susceptibility of ice formation in upper tropospheric clouds to insoluble aerosol components, *J. Geophys. Res.*, *102*, 19,575–19,584.

DeMott, P. J., Y. Chen, S. M. Kreidenweis, D. C. Rogers, and D. E. Shermann (1999), Ice formation by black carbon particles, *Geophys. Res. Lett.*, *26*, 2429–2432.

DeMott, P. J., K. Sassen, M. R. Poellot, D. Baumgardner, D. C. Rogers, S. D. Brooks, A. J. Prenni, and S. M. Kreidenweis (2003), African dust aerosols as atmospheric ice nuclei, *Geophys. Res. Lett.*, *30*(14), 1732, doi:10.1029/2003GL017410.

Dowling, D. R., and L. F. Radke (1990), A summary of the physical-properties of cirrus clouds, *J. Appl. Meteorol.*, *29*, 970–978.

Dymarska, M., B. J. Murray, L. Sun, M. L. Eastwood, D. A. Knopf, and A. K. Bertram (2006), Deposition ice nucleation on soot at temperatures relevant for the lower troposphere, *J. Geophys. Res.*, *111*, D04204, doi:10.1029/2005JD006627.

Gettelman, A., W. D. Collins, E. J. Fetzer, A. Eldering, F. W. Irion, P. B. Duffy, and G. Bala (2006), Climatology of upper tropospheric relative humidity from the atmospheric infrared sounder and implications for climate, *J. Clim.*, *19*(23), 6104–6121.

Gierens, K. (2003), On the transition between heterogeneous and homogeneous freezing, *Atmos. Chem. Phys.*, *3*, 437–446.

Ginoux, P., M. Chin, I. Tegen, J. M. Prospero, B. Holben, O. Dubovik, and S.-J. Lin (2001), Sources and distributions of dust aerosols simulated with the GOCART model, *J. Geophys. Res.*, *106*, 20,255–20,274.

Gong, S. L., L. A. Barrie, and J.-P. Blanchet (1997), Modeling sea-salt aerosols in the atmosphere: 1. Model development, *J. Geophys. Res.*, *102*, 3805–3818.

Guenther, A., et al. (1995), A global model of natural volatile organic compound emissions, *J. Geophys. Res.*, *100*, 8873–8892.

Haag, W., B. Karcher, J. Strom, A. Minikin, U. Lohmann, J. Ovarlez, and A. Stohl (2003), Freezing thresholds and cirrus cloud formation mechanisms inferred from in situ measurements of relative humidity, *Atmos. Chem. Phys.*, *3*, 1791–1806.

Haag, W., and B. Kärcher (2004), The impact of aerosols and gravity waves on cirrus clouds at midlatitudes, *J. Geophys. Res.*, *109*, D12202, doi:10.1029/2004JD004579.

Hack, J. J., et al. (2006), Simulation of the global hydrological cycle in the CCSM Community Atmospheric Model Version 3 (CAM3): Mean features, *J. Clim.*, *16*, 2199–2221.

Hendricks, J., B. Kärcher, A. Döpelheuer, J. Feichter, U. Lohmann, and D. Baumgardner (2004), Simulating the global atmospheric black carbon cycle: A revisit to the contribution of aircraft emissions, *Atmos. Chem. Phys.*, *4*, 2521–2541.

Hendricks, J., B. Kärcher, U. Lohmann, and M. Ponater (2005), Do aircraft black carbon emissions affect cirrus clouds on the global scale?, *Geophys. Res. Lett.*, *32*, L12814, doi:10.1029/2005GL022740.

Heymsfield, A., et al. (2005), *The Ice in Clouds Experiment-Research Plan*, Scientific Overview Document, National Center for Atmospheric Research, September 2, 2005. (Available at http://www.mmm.ucar.edu/events/ice05/images/ICE-SOD-050902.pdf)

Hoyle, C. R., B. P. Luo, and T. Peter (2005), The origin of high ice crystal number densities in cirrus clouds, *J. Atmos. Sci.*, *62*, 2568–2579.

Ito, A., and J. E. Penner (2005), Historical emissions of carbonaceous aerosols from biomass and fossil fuel burning for the period 1870–2000, *Global Biogeochem. Cycles*, *19*(2), GB2028, doi:10.1029/2004GB002374.

Jacobson, M. Z. (2003), Development of mixed-phase clouds from multiple aerosol size distributions and the effect of the clouds on aerosol removal, *J. Geophys. Res.*, *108*(D8), 4245, doi:10.1029/2002JD002691.

Jensen, E. J., and L. Pfister (2004), Transport and freeze-drying in the tropical tropopause layer, *J. Geophys. Res.*, *109*, D02207, doi:10.1029/2003JD004022.

Jensen, E. J., O. B. Toon, D. L. Westphal, S. Kinne, and A. J. Heysmfield (1994), Microphysical modeling of cirrus: 1. Comparison with 1986 fire IFO measurements, *J. Geophys. Res.*, *99*, 10,421–10,442.

Jensen, E. J., L. Pfister, A. S. Ackerman, A. Tabazadeh, and O. B. Toon (2001), A conceptual model of the dehydration of air due to freeze drying by optically thin, laminar cirrus rising slowly across the tropical tropopause, *J. Geophys. Res.*, *106*, 17,237–17,253.

Kärcher, B. (2004), Cirrus clouds in the tropical tropopause layer: Role of heterogeneous ice nuclei, *Geophys. Res. Lett.*, *31*, L12101, doi:10.1029/2004GL019774.

Kärcher, B., and U. Lohmann (2002a), A parameterization of cirrus cloud formation: Homogeneous freezing of supercooled aerosols, *J. Geophys. Res.*, *107*(D2), 4010, doi:10.1029/2001JD000470.

Kärcher, B., and U. Lohmann (2002b), A parameterization of cirrus cloud formation: Homogeneous freezing including effects of aerosol size, *J. Geophys. Res.*, *107*(D23), 4698, doi:10.1029/2001JD001429.

Kärcher, B., J. Hendricks, and U. Lohmann (2006), Physically based parameterization of cirrus cloud formation for use in global atmospheric models, *J. Geophys. Res.*, *111*, D01205, doi:10.1029/2005JD006219.

Kärcher, B., O. Möhler, P. J. DeMott, S. Pechtl, and F. Yu (2007), Insights into the role of soot aerosols in cirrus cloud formation, *Atmos. Chem. Phys.*, *7*, 4203–4227.

Kettle, A. J., and M. O. Andreae (2000), Flux of dimethylsulfide from the oceans: A comparison of updated data seas and flux models, *J. Geophys. Res.*, *105*, 26,793–26,808.

Kinne, S., et al. (2006), An AeroCom initial assessment - optical properties in aerosol component modules of global models, *Atmos. Chem. Phys.*, *6*, 1815–1834.

Koop, T., B. P. Luo, A. Tsias, and T. Peter (2000), Water activity as the determinant for homogeneous ice nucleation in aqueous solutions, *Nature*, *406*, 611–614.

Liou, K. N. (1986), Influence of cirrus clouds on weather and climate processes: A global perspective, *Mon. Weather Rev.*, *114*, 1167–1199.

Liu, X., and J. E. Penner (2005), Ice nucleation parameterization for global models, *Meteorol. Zeitschr.*, *14*, 499–514.

Liu, X. H., J. E. Penner, and M. Herzog (2005), Global modeling of aerosol dynamics: Model description, evaluation, and interactions between sulfate and nonsulfate aerosols, *J. Geophys. Res.*, *110*(D18), D18206, doi:10.1029/2004JD005674.

Liu, X., J. E. Penner, S. Ghan, and M. Wang (2007a), Inclusion of ice microphysics in the NCAR Community Atmospheric Model version 3 (CAM3), *J. Clim.*, *20*, 4526–4547.

Liu, X., S. Xie, and S. J. Ghan (2007b), Evaluation of a new mixed-phase cloud microphysics parameterization with CAM3 single-column model and M-PACE observations, *Geophys. Res. Lett.*, *34*, L23712, doi:10.1029/2007GL031446.

Lohmann, U. (2002), Possible aerosol effects on ice clouds via contact nucleation, *J. Atmos. Sci.*, *59*, 647–656.

Lohmann, U., and B. Kärcher (2002), First interactive simulations of cirrus clouds formed by homogeneous freezing in the ECHAM general circulation model, *J. Geophys. Res.*, *107*(D10), 4105, doi:10.1029/2001JD000767.

Lohmann, U., B. Kärcher, and J. Hendricks (2004), Sensitivity studies of cirrus clouds formed by heterogeneous freezing in the ECHAM GCM, *J. Geophys. Res.*, *109*, D16204, doi:10.1029/2003JD004443.

McFarquhar, G. M., J. Um, M. Freer, D. Baumgardner, G. L. Kok, and G. G. Mace (2007), The importance of small ice crystals to cirrus properties: Observations from the Tropical Warm Pool International Cloud Experiment (TWP-ICE), *Geophys. Res. Lett.*, *34*, L13803, doi:10.1029/2007GL029865.

Meyers, M. P., P. J. DeMott, and W. R. Cotton (1992), New primary ice nucleation parameterizations in an explicit cloud model, *J. Appl. Meteorol.*, *31*, 708–721.

Ming, Y., V. Ramaswamy, L. J. Donner, and V. T. J. Phillips (2007), Modeling the interactions between aerosols and liquid water clouds with a self-consistent cloud scheme in a general circulation model, *J. Atmos. Sci.*, *64*, 1189–1209.

Minikin, A., A. Petzold, J. Ström, R. Krejci, M. Seifert, P. van Veltoven, H. Schlager, and U. Schumann (2003), Aircraft observations of the upper tropospheric fine particle aerosol in the Northern and Southern Hemispheres at midlatitudes, *Geophys. Res. Lett.*, *30*(10), 1503, doi:10.1029/2002GL016458.

Mitchell, D., et al. (2008), Impact of small ice crystal assumptions on ice sedimentation rates in cirrus clouds and GCM simulations, *Geophys. Res. Lett.*, *35*, L09806, doi:10.1029/2008GL033552.

Möhler, O., et al. (2005a), Effect of sulfuric acid coating on heterogeneous ice nucleation by soot aerosol particles, *J. Geophys. Res.*, *110*, D11210, doi:10.1029/2004JD005169.

Möhler, O., C. Linke, H. Saathoff, M. Schnaiter, R. Wagner, A. Mangold, M. Kramer, and U. Schurath (2005), Ice nucleation on flame soot aerosol of different organic carbon content, *Meteorol. Zeitschr.*, *14*, 477–484.

Moritz, R. E., C. M. Bitz, and E. J. Steig (2002), Dynamics of recent climate change in the Arctic, *Science*, *297*, 1497–1502.

Murphy, D. M., D. J. Cziczo, K. D. Froyd, P. K. Hudson, B. M. Matthew, A. M. Middlebrook, R. E. Peltier, A. Sullivan, D. S. Thomson, and R. J. Weber (2006), Single-particle mass spectrometry of tropospheric aerosol particles, *J. Geophys. Res.*, *111*, D23S32, doi:10.1029/2006JD007340.

Nedoluha, G. E., et al. (2003), An evaluation of trends in middle atmospheric water vapor as measured by HALOE, WVMS, and POAM, *J. Geophys. Res.*, *108*(D13), 4391, doi:10.1029/2002JD003332.

Notholt, J., et al. (2005), Influence of tropospheric $SO_2$ emissions on particle formation and the stratospheric humidity, *Geophys. Res. Lett.*, *32*, L07810, doi:10.1029/2004GL022159.

Oltmans, S. J., H. Vomel, D. J. Hofmann, K. H. Rosenlof, and D. Kley (2000), The increase in stratospheric water vapor from balloonborne frost point hygrometer measurements at Washington, D. C., and Boulder, Colorado, *Geophys. Res. Lett.*, *27*, 3453–3456.

Penner, J. E., Y. Chen, M. Wang, and X. Liu (2008), Possible influence of anthropogenic aerosols on cirrus clouds and anthropogenic forcing, *Atmos. Chem. Phys.*, in press.

Petzold, A., and F. P. Schröder (1998), Jet engine exhaust aerosol characterization, *Aerosol Sci. Technol.*, *28*, 62–76.

Petzold, A., A. Döpelheuer, C. A. Brock, and F. P. Schröder (1999), In situ observations and model calculations of black carbon emission by aircraft at cruise altitude, *J. Geophys. Res.*, *104*, 22,171–22,181.

Pruppacher, H. R., and J. D. Klett (1997), *Microphysics of Cloud and Precipitation*, 954 pp., Springer, New York.

Pueschel, R. F., D. F. Blake, K. G. Snetsinger, A. D. A. Hansen, S. Verma, and K. Kato (1992), Black carbon (soot) aerosol in the lower stratosphere and upper troposphere, *Geophys. Res. Lett.*, *19*, 1659–1662.

Rahmes, T. F., A. H. Omar, and D. J. Wuebbles (1998), Atmospheric distributions of soot particles by current and future aircraft fleets and resulting radiative forcing on climate, *J. Geophys. Res.*, *103*, 31,657–31,667.

Ramanathan, V., and W. Collins (1991), Thermodynamics regulation of ocean warming by cirrus clouds deduced from observations of the 1987 El Nino, *Nature*, *357*, 24–32.

Rasch, P., and J. E. Kristjánsson (1998), A comparison of the CCM3 model climate using diagnosed and predicted condensate parameterizations, *J. Clim.*, *11*, 1587–1614.

Rosenlof, K. H., et al. (2001), Stratospheric water vapor increases over the past half-century, *Geophys. Res. Lett.*, *28*, 1195–1198.

Rossow, W. B., and R. A. Schiffer (1999), Advances in understanding clouds from ISCCP, *Bull. Am. Metereol. Soc.*, *80*, 2261–2286.

Rotstayn, L. D., B. F. Ryan, and J. J. Katzfey (2000), A scheme for calculation of the liquid fraction in mixed-phase stratiform clouds in large-scale models, *Mon. Weather Rev.*, *128*, 1070–1088.

Sanderson, B. M., C. Piani, W. J. Ingram, D. A. Stone, and M. R. Allen (2008), Towards constraining climate sensitivity by linear analysis of feedback patterns in thousands of perturbed-physics GCM simulations, *Clim. Dyn.*, *30*, 175–190.

Sassen, K., and G. C. Dodd (1988), Homogeneous nucleation rate for highly supercooled cirrus cloud droplets, *J. Atmos. Sci.*, *45*, 1357–1369.

Schulz, M., et al. (2006), Radiative forcing by aerosols as derived from the AeroCom present-day and pre-industrial simulations, *Atmos. Chem. Phys.*, *6*, 5225–5246.

Schumann, U. (2002), Contrails cirrus, in *Cirrus*, edited by D. K. Lynch et al., pp. 231–255, Oxford Univ. Press, Oxford, U.K.

Sherwood, S. (2002), A microphysical connection among biomass burning, cumulus clouds, and stratospheric moisture, *Science*, *295*, 1272–1275.

Smith, W. L., S. Ackerman, H. Revercomb, H. Huang, D. H. DeSlover, W. Feltz, L. Gumley, and A. Collard (1998), Infrared spectral absorption of nearly invisible cirrus clouds, *Geophys. Res. Lett.*, *25*, 1137–1140.

Smith, S., R. Andres, L. Conception, and J. Lurz (2004), Historical sulfur dioxide emissions 1850–2000: Methods and results, *JGCRI Research Report PNNL* 14537, 16 pp., Pacific Northwest National Laboratory, Wa. (Available at http://www.pnl.gov/main/pulications/external/technical_reports/PNNL 14537.pdf)

Stephens, G. L., S. C. Tsay, P. W. Stackhouse, and P. J. Flatau (1990), The relevance of the microphysical and radiative properties of cirrus clouds to climate and climatic feedback, *J. Atmos. Sci.*, *47*, 1742–1753.

Strawa, A. W., et al. (1999), Carbonaceous aerosol (Soot) measured in the lower stratosphere during POLARIS and its role in stratospheric photochemistry, *J. Geophys. Res.*, *104*, 26,753–26,766.

Ström, J., and S. Ohlsson (1998), In situ measurements of enhanced crystal number densities in cirrus clouds caused by aircraft exhaust, *J. Geophys. Res.*, *103*, 11,355–11,361.

Textor, C., et al. (2006), Analysis and quantification of the diversities of aerosol life cycles within AeroCom, *Atmos. Chem. Phys.*, *6*, 1777–1813.

Thompson, D. W. J., and J. M. Wallace (2001), Regional climate impacts of the Northern Hemisphere annular mode and associated climate trends, *Science*, *293*, 85–89.

Travis, D. J., A. M. Carleton, and R. G. Lauritsen (2002), Contrails reduce daily temperature range, *Nature*, *418*, 6012002.

Xie, S., J. Boyle, S. A. Klein, X. Liu, and S. J. Ghan (2008), Simulations of Arctic mixed-phase clouds in forecasts with CAM3 and AM2 for M-PACE, *J. Geophys. Res.*, *113*, D04211, doi:10.1029/2007JD009225.

Wang, P.-H., P. Minnis, M. P. McCormick, G. S. Kent, and K. M. Skeens (1996), A 6-year climatology of cloud occurence frequency from Stratospheric Aerosol and Gas experiment II observations (1985–1990), *J. Geophys. Res.*, *101*, 29,407–29,429.

Young, K. C. (1974), The role of contact nucleation in ice phase initiation in clouds, *J. Atmos. Sci.*, *31*, 768–776.

Zhang, Y. (2008), Online-coupled meteorology and chemistry models: History, current status, and outlook, *Atmos. Chem. Phys.*, *8*, 2895–2932.

Zhang, M., W. Lin, C. B. Bretherton, J. J. Hack, and P. J. Rasch (2003), A modified formulation of fractional stratiform condensation rate in the NCAR Community Atmosphere Model (CAM2), *J. Geophys. Res.*, *108*(D1), 4035, doi:10.1029/2002JD002523.

X. Liu, Atmospheric Science and Global Change Division, Pacific Northwest National Laboratory, 3200 Q Avenue, MSIN K9-24, Richland, WA 99352, USA. (xiaohong.liu@pnl.gov)

J. E. Penner and M. Wang, Department of Atmospheric, Oceanic and Space Sciences, Space Research Building, University of Michigan, 2455 Hayward Street, Ann Arbor, MI 48109-2143, USA.